SLAC–PUB–4993
October 1989
(I/E)

THE LIMITED STREAMER TUBES OF THE SLD *

A. C. BENVENUTI
INFN, Sezione di Bologna, I–40126 Bologna, Italy

L. PIEMONTESE
INFN, Sezione di Ferrara and Università di Ferrara, I–44100 Ferrara, Italy

A. CALCATERRA, R. DE SANGRO, P. DE SIMONE, I. PERUZZI and M. PICCOLO
Lab. Nazionali di Frascati dell'INFN, I-00044 Frascati (Roma), Italy

P. N. BURROWS, W. BUSZA, S. L. CARTWRIGHT, J. I. FRIEDMAN, S. FUESS, S. GONZALEZ, T. HANSL-KOZANECKA, H. W. KENDALL, A. LATH, T. LYONS, L. S. OSBORNE, L. ROSENSON, U. SCHNEEKLOTH, F. E. TAYLOR, R. VERDIER, D. WILLIAMS and J. M. YAMARTINO
Massachusetts Institute of Technology, Cambridge, MA 02139, USA

N. BACCHETTA, D. BISELLO, A. CASTRO, M. LORETI, L. PESCARA and J. WYSS
INFN, Sezione di Padova and Università di Padova, I-35100 Padova, Italy

B. ALPAT, R. BATTISTON, G. M. BILEI, R. DELL'ORSO, G. MANTOVANI, M. PĀULUZZI and L. SERVOLI
INFN, Sezione di Perugia and Università di Perugia, I-06100 Perugia, Italy

M. CARPINELLI, R. CASTALDI, C. VANNINI and P. G. VERDINI
INFN, Sezione di Pisa and Università di Pisa, I-56010 San Piero a Grado, Italy

B. L. BYERS, D. KHARAKH, R. L. MESSNER and R. W. ZDARKO
Stanford Linear Accelerator Center, Stanford University, Stanford, CA 94309, USA

J. R. JOHNSON
University of Wisconsin, Madison, WI 53706, USA

Abstract

A large hadron calorimeter and muon tracking device using plastic streamer tubes has been constructed in the iron flux-return structure for the SLD detector at SLAC. Various studies of the operating characteristics of the streamer tubes of this system are presented. Emphasis is placed on the tracking capabilities of the device and on the optimization of the high voltage and readout electronics.

Submitted to Nuclear Instruments and Methods A.

*Work supported in part by Department of Energy (USA) contracts DE–AC02–76ER03069 (MIT), DE–AC03–76SF00515 (SLAC), and DE–AC02–76ER00881 (UW), and by the Istituto Nazionale di Fisica Nucleare (Italy).

1. Introduction

A new detector (SLD) is being constructed at SLAC to study e^+e^- physics in the Z^0 mass range [1]. The calorimetry of the experiment will be performed by a Liquid Argon Calorimeter (LAC), consisting at normal incidence of about 2.7 absorption lengths (λ), placed inside the magnet coil (0.69 λ); and by a set of limited streamer tubes [2], called the Warm Iron Calorimeter (WIC), placed outside the magnet coil in the iron flux-return structure. The WIC functions primarily as a "tail catcher" by measuring the energy which escapes the liquid argon calorimeter and the coil. Since the energy deposited in a hadronic shower has large fluctuations in the longitudinal direction, the limited streamer calorimeter is an important component of the SLD calorimeter system and its proper function is necessary to achieve good energy resolution.

The total number of absorption lengths, λ_{total}, in the SLD calorimeter is about 7.8 for normal incidence in the barrel. The total absorber thickness is slightly smaller for the endcaps where $\lambda_{total} = 7.1$. The calorimetry system is designed with fine segmentation both laterally and longitudinally. The WIC samples the shower every 0.5 λ longitudinally behind the roughly 3.4 λ of the LAC and the coil. The lateral sampling of the WIC is performed in projective towers approximately $\Delta\theta_{polar} \times \Delta\Phi_{azimuth} = 66$ mr $\times 66$ mr from the e^+e^- collision point. The towers are broken into two roughly equal longitudinal segments.

A second function of the chambers is to identify and track muons. The chambers are constructed with a digital readout by means of electrical pickup strips placed parallel (and in some cases perpendicular) to the wires of the limited streamer tubes. With these parallel strips a spatial resolution of about $\sigma \approx 0.3$ cm is achieved.

Figure 1 shows the iron structure of the SLD. All of the magnetic flux return iron of both the central region (the "barrel") and the endcap region is instrumented with limited streamer tubes. Roughly 4500 sq m of these tubes have been constructed.

In a companion paper [3], we described the fabrication of the tubes and their assembly into chambers which can sample hadron shower energy and identify and measure muon tracks. Here we report on various measurements we performed to understand the basic operation of the tubes to ensure that the functions of calorimetry, muon identification and tracking are achieved.

The specific issues addressed in this paper are:

1. Investigations of the limited streamer discharge mechanism.
2. Design of the high voltage circuit and its relation to calorimetry and muon tracking.
3. Operating characteristics of the digital tracking and analog readout.
4. Choice of the operating point and its stability.
5. Life tests of the modules.

2. Mechanical and electrical fundamentals

The basic construction unit of the limited streamer tubes is a group of eight "U"-shaped channels employing a single piece of extruded PVC plastic, with an anode wire strung in each channel. This wire-U-channel assembly is inserted in a gas-tight envelope, also made from inexpensive PVC plastic, to form a "module." Approximately 10,000 of these modules, ranging in length from 1.9 to 8.6 m, have been constructed. The open channels, forming the cells of a module, are 9 mm wide by 9 mm deep separated by 1-mm-thick walls with a 1-mm-thick bottom. Molded plastic pieces with electrical and gas penetrations are inserted at the ends of the plastic envelope to provide high voltage (HV) and ground connections and to complete the gas system. The anode wires are of 100 μm diameter silver-lubricated beryllium-copper and are supported every 40 cm along the profile by plastic "bridges." Electrical isolation between the individual wires of a module is provided by soldering each anode wire to a 220 Ω series resistor which in turn is connected to the HV bus. This resistor-bus assembly is constructed on a small G–10 card (a ceramic card was used in the early production modules) and is inserted in the gas envelope at the end of the module. Figure 2 shows a cutaway view of a module.

The extruded plastic profiles are coated with a layer of conducting graphite paint to form the cathode of the limited streamer tube. The surface resistivity ranged from 0.05 to 2.0 MΩ/sq. An extra coating of low resistivity graphite paint was added to the tops of the PVC U–channels to reduce the high electric fields which may exist around small discontinuities of the original graphite coating. A typical end-to-end resistance of a 6 m profile (within rather wide limits) is about 3 MΩ with no additional coating, and 200 kΩ with the extra coating. Care was taken to make the surface resistance high enough to allow the limited streamer discharge to be picked up capacitively by external electrodes mounted on the outside of the gas envelope, yet small enough to provide a uniform electrical field with no spurious discharges arising from isolated carbon particles on the surface [4]. Further details of the construction can be found in our companion paper [3].

As constructed, a cell of a limited streamer module forms an open-ended transmission line with a capacitance per unit length $\approx$ 12 pF/m, and inductance per unit length 1 μH/m, resulting in a characteristic impedance $Z = \sqrt{L/C} \approx 290\ \Omega$. The unterminated configuration has the property that a positive (same sign) reflection of the anode pulse takes place at the open end (the end opposite the HV connection) of the transmission line. The pulse on the anode wire travels at nearly the speed of light, which in a tube of a few meters length gives rise to pulse delays that are longer than the pulse rise time. This behavior is displayed in fig. 3, where we note that pulses on the anode wire induced by streamers far from the HV connection are single-lobed, whereas pulses from streamers near the HV end are double-lobed and have about one-half the pulse height of the far pulses. The time separation of the two lobes is consistent with the round trip propagation time.

The modules are read out by means of external electrodes mounted on the outside of the gas envelope. The muon tracking readout of the chambers is performed by narrow copper strips approximately 8 mm wide, which are cut from copper foil on a fiberglass sheet laminated to the modules so that they are aligned parallel to the wires (called "x–strips"). An orthogonal coordinate measurement is obtained in certain chamber layers by readout strips 4 cm wide (2 cm in the endcaps) cut perpendicular to the wires (called "y–strips"). The x–strips are fastened to the closed side of the PVC U–channels, thus requiring the induced pulse to penetrate the graphite coated PVC bottom. The y–strips are mounted on the open side of the U–channels. The calorimetry is performed by detecting the integrated charge induced on quadrilateral pads attached outside the gas-tight housing on the open side of the U–channels, except when there are y–strips on the same layer.

The chamber construction is shown in fig. 4. Indicated in the figure are the placement of the strip and pad readout planes, the connection of the pads to a readout transmission line (for the endcaps only), and the outer ground planes which are tied together at the edges of the chamber to provide an overall electrical shield. The outer ground plane on the strip side also acts as the ground side of a transmission line formed between the x–strips and itself. The ground reference for the strip and pad pulse readout is this outer ground.

Not shown in the figure is the detail that the endcap chambers are constructed with an additional plastic sleeve, similar to but slightly larger than the gas PVC envelope to locate the modules in the chambers. This double sleeve innovation allows defective modules to be replaced without delaminating the entire chamber and enables the construction of the chamber to be decoupled from the modules.

3. The limited streamer mechanism

Here we review some aspects of the limited streamer discharge mechanism which have guided our choice of the operating point of the chambers.

If the amplitude of the pulses on the anode wire is plotted as a function of the anode voltage, one finds that as the voltage is increased the anode pulse amplitude undergoes a rapid transition from a regime where the pulse charge is roughly proportional to the initial ionization (so-called "proportional mode") to a mode of operation where the charge is roughly independent of the input ionization (called the "limited streamer mode"). Evidence has been presented to show that the discharge takes place over a small region of the wire, and does not extend the entire distance between the anode and the cathode [5]. The limited streamer mechanism is distinguished from the Geiger–Müller mode where a discharge along the entire anode wire takes place. The effect is observed chiefly in "thick" wires > 40 μm in diameter, and in heavily quenched gases, such as 25% argon–75% isobutane. The limited streamer mode is capable of operation at kilohertz rates. The attribute of large pulse height produced by the limited streamer chamber is one of the chief attractions of this device, making the chamber easy to operate and the readout electronics comparatively easy to construct.

Figure 5 shows the peak value of the charge integrated on the anode wire (50 μm and 100 μm diameter) as a function of the anode–cathode high voltage. A ^{106}Ru source illuminated the chambers which were filled with a 25% argon–75% isobutane gas mixture by volume. The gas mixture was fixed by a mass-flow gas control system [6] and was monitored by a gas chromatograph [7]. A LeCroy QVT [8] was used with a 500 ns gate to record the data. The transition between the proportional mode and the limited streamer mode is quite evident. Similar data have been taken with cosmic rays indicating roughly the same charge per pulse as a function of HV and the same sudden transition from the proportional mode to the limited streamer mode.

The proportional mode and the limited streamer mode are well separated in the 100 μm wire data and are observed to coexist in the HV range of 4.4 kV to 4.6 kV. No such coexistence of the two modes is observed in the 50 μm data, which we attribute to the observation (see fig. 5) that the proportional mode in the 50 μm wire has a relatively higher gain with respect to the limited streamer mode at the transition voltage than in the 100 μm wire.

A close examination of the two operating modes shows that the proportional mode for both wire diameters has the characteristic exponential HV behavior [9] roughly given by:

$$Q(V) \;=\; Q_0 \;\exp\left\{\kappa\sqrt{\frac{V}{V_{Tp}}}\left(\sqrt{\frac{V}{V_{Tp}}}-1\right)\right\} \;\approx\; Q_0 \;\exp\left\{\kappa\frac{V}{V_{Tp}}\right\} \quad , \qquad (1)$$

where $Q(V)$ is the anode charge developed with applied anode voltage V; Q_0 is the initial ionization (electrons); κ is a constant which depends on the critical electrical field, gas constants, and the radius of the anode wire; and V_{Tp} is the threshold voltage for the proportional mode. In contrast, the limited streamer mode shows a linear dependence on the anode–cathode voltage given by:

$$Q(V) \approx \beta(V - V_{Tls}) \quad , \tag{2}$$

where β is a constant which is dependent on the wire diameter, and V_{Tls} is the parametric transition voltage marking the onset of the limited streamer mode. The transition voltage is dependent on the gas composition, temperature, and pressure.

The linear HV dependence of the integrated anode charge is expected if the gas discharge is controlled by space charge effects which limit the charge multiplication in the avalanche. The large charge buildup in the streamer will partially cancel the anode–cathode electric field and thus contributes to the quenching of the streamer. Corroboration of this view is found by noting that a typical anode pulse charge in the present experiment is about 25 pC, corresponding to about 1.3×10^8 electrons, close to the Raether condition [10] where space charge effects are expected to become important.

Since we want to operate the chambers in the limited streamer mode, we have chosen the 100 μm diameter wire over the 50 μm wire. The 100 μm wire is mechanically more robust than the 50 μm wire, making the construction and handling of the modules easier. In the case of the 100 μm wire, the proportional mode and the limited streamer mode are well separated over a wide range of mixtures of argon and isobutane. In fig. 6, we show the pulse height spectra as a function both of the HV and the proportions of this binary gas mixture. The plot clearly indicates that the transition point between the proportional and the limited streamer modes moves to higher voltage as the argon content is reduced. Nevertheless, a clear separation of the two modes is evident for an argon fraction greater than 20%.

Figure 7 shows the general trend of the average pulse height as a function of high voltage and gas composition for both the limited streamer [fig. 7(a)] and the proportional modes [fig. 7(b)]. In fig. 7(c) we plot the concomitant fraction of the pulses attributed to the limited streamer mode where the two modes are distinguishable. We note that in most of the regions where the two modes coexist, the limited streamer mode gain is roughly a factor of 10 larger than the proportional mode gain.

Atac et al. [5] have photographed limited streamers in an argon (50%)–ethane (50%) mixture. They found that the streamers are filaments, typically 150 to 200 μm wide extending along the electric field lines, which grow with increasing HV to about a few millimeters from the anode wire. We expect that similar dimensions appertain to other gases; in particular, to the isobutane (75%)–argon (25%), ["3:1 gas"], or the nonflammable gas mixture of isobutane (9.5%)–argon (2.5%)–CO_2 (88%) ["three-component gas"] which we have studied [11].

An indirect measure of the extended nature of the streamers is obtained by plotting the charge accumulated on the pads versus the sum of the charge collected on the strips [12]. Each external readout electrode (the sum of the pads or the sum of the strips) subtends roughly one-half of the total solid angle from the streamer. (The sum of the strips subtends roughly 2π steradians from the streamer, whereas the strip immediately below the wire subtends roughly π steradians.) We therefore expect that each (sum) electrode will accumulate about one-half of the absolute magnitude of the anode charge. This we find to be approximately true. Figure 8 shows the correlation of the sum of the charges accumulated on the pads and strips versus the charge detected on the anode wire. The plot indicates a tight correlation between these pulse heights.

However, if the charge picked up on the sum of the strips and the sum of the pads are examined separately we become sensitive to the geometric fluctuations of the individual streamers. For example, when the streamer is closer to the strip side we expect that the strips will accumulate more charge, and vice versa. Therefore, the fluctuation of the pad charge versus the sum strip charge is indicative of the spatial extent of the streamers. Figure 9 shows the pad charge versus the summed strip charge. We note that for small pulse heights, corresponding to the proportional mode where the gas amplification is confined to a narrow region about the anode wire, the sum-strip charge is closely correlated to the pad charge. Larger charges from the limited streamers exhibit a looser correlation arising from the larger spatial extent of the ionization of the limited streamers. These intrinsic geometric fluctuations are a contribution to the pulse height resolution of the strip and pad readouts, but are dominated by the fluctuations of the streamer formation itself.

Other gases, such as the nonflammable three-component gas that we have developed [11], show the same lack of correlation observed in the more heavily quenched isobutane 3:1 gas mixture. Figure 10 is a plot of the pad versus sum-strip correlation for this gas.

4. Design of the HV circuit

To achieve the dual purpose of good muon tracking and hadron calorimetry, we have designed the HV circuit to minimize strip-to-strip cross-talk while ensuring that the calorimetry will be reliable. These goals impose the following requirements:

1. The signal on the strips other than the one over the struck wire is to be minimized.
2. The operating point of the limited streamer chambers should not shift when large charge loads are imposed, such as during the energy deposition of a high energy shower.

3. Module HV connections should be isolated from each other to eliminate electrical cross-talk.

4. A means of monitoring the average current drawn by each module should be available.

5. The possibility of pulsing the wires of a module to check the strip and pad readout should exist.

The essentials of the HV hookup which satisfy these requirements are shown in fig. 11. The elements enclosed within the dotted line in the figure are mounted on the "HV-board." Other elements of the HV circuit are mounted on the module itself. Each module is connected to a 2 nF HV-clamping capacitor in series with an individual 150 Ω resistor connected to a common pulser bus having a single common 5 Ω resistor to ground. This arrangement enables the wires of the modules to be pulsed with an external pulse generator to simulate the operation of the tubes. Isolation from the HV power supply and other modules is provided by 20 MΩ series resistors. The cathode of each tube (the graphite-coated wall of the PVC profile) is connected to ground through a 10 kΩ resistor with a 10 nF bypass capacitor, allowing the current drawn by each module to be measured at the indicated test point. The 10 nF capacitor ensures that the effective resistance of the ground return for pulses is determined by the resistive cathode rather than by the HV circuit. The isolation of the individual wires within a module is achieved by 220 Ω series resistors mounted on a G–10 card inserted at the end of the module within the gas envelope as mentioned above.

The immediate source of charge for the limited streamer tube pulses is that stored in the tube itself by the cell capacitance $C \approx 12$ pF/m, typically about 60 nC/m. The sag in the anode–cathode voltage is limited to $\leq 1\%$ for up to 60 streamers in a

6-m-long tube. This is larger than the expected charge demand for a given cell. The 2 nF capacitor connected to each module (shared by all eight cells of a module) maintains the anode–cathode voltage by providing a large ballast charge. This capacitor further allows the anode wire pulse to be absorbed in a characteristic resistance to minimize reflections. The particular choice of the 150 Ω resistor was the result of a study of the strip-to-strip cross-talk and will be discussed in the next section.

The strip and pad readouts

The chambers are constructed so that the pad electrodes used in the calorimetry measurement and the y–strips (transverse to the wires) are on the open side of the profile, and the x–strips (parallel to the wires), which are used for the muon tracking, are on the closed side of the profile. Figures 2 and 4 show the construction of the modules and the chambers, respectively. Note that the x–strip readout is always connected on the end away from the HV connection. Because of the open-profile construction of the limited streamer tubes, the efficiency for streamer formation by penetrating particles is reduced by the dead space occupied by the walls of the profile. This limits the maximum attainable efficiency to 92% for normal incidence.

Pulses are induced on the external electrodes primarily by the electric field associated with the positive ion column of the limited streamer discharge. The formation time of the limited streamer is of the order of nanoseconds so the capacitive coupling to the external electrodes is large. Given the polarity of this electric field, the induced pulses on the external electrodes will be initially positive going. For times less than the 100 μsec needed for the positive ions to drift from the anode to the cathode, the charge of the pulse on the external electrodes will be proportional to the total charge of the streamer collected on the anode wire.

5.1. *The x–strip readout*

The x–strips are external electrodes mounted parallel to the anode wires so that there is one strip per wire, although some special chambers in the endcap were built with two wires per strip. Various models have been proposed to describe the characteristics of the x–strip readout, such as the L-C-R model of Battistoni et al., [13] or the model of Kajino et al., [14]. However, since the chambers in our experiment have long modules, typically 6 to 7 m, we have modeled the equivalent circuit of the x–strip readout as a set of transmission lines.

The excitation of the transmission line is caused by the distortion of the electric field between the anode and the resistive cathode by the streamer. Referring to fig. 12, we note that there are basically two transmission lines in the circuit. The first transmission line is formed between the wire and a given strip and has a characteristic impedance $Z_1 \approx 400\ \Omega$. The resistive cathode plane lies between the wire and the strip, but is of high impedance and does not interfere very much with the signal in the wire-strip transmission line. The second transmission line of the equivalent circuit is formed between the strip and the external ground plane and has a characteristic impedance $Z_2 \approx 33\ \Omega$. The strip readout electronics is matched to this impedance although it is connected to the strip transmission line through a short (<1 m) flat cable of impedance $\approx 80\ \Omega$. The wire of the first transmission line is connected to the second transmission line by the series combination of the 220 Ω resistor on the G–10 card, the 150 Ω terminating resistor in the HV circuit, and the HV clamping (blocking) capacitor to the common ground.

Because the two transmission lines share a common conductor, we expect to observe the same dependence of the pulse shape on the position of the streamer in the strip-ground transmission line as observed on the anode wire-strip line. This is shown in fig. 13, where we compare the pulse shape on the anode wire with that on the x–strip line. Note that when the streamer is formed near the HV input [fig. 13(b)], the x–strip pulse is double-lobed from the open-ended reflection in the same manner as the anode wire pulse. When the streamer is far from the HV connection [fig. 13(a)], both the strip and the anode pulse are approximately single-lobed.

This behavior has important consequences in achieving spatial uniformity of the strip readout. If the strip electronics is voltage sensing, then for efficient operation the discriminator level has to be set to accommodate the smallest pulse amplitude, i.e., the case when the streamer is close to the HV input. A charge-sensitive discriminator, on the other hand, is not sensitive to this spatial variation since the charge of the double-lobed pulse is the same as the single-lobed one. The dependence of the efficiency on the position of the streamer along the tube is shown in fig. 14 for a voltage-sensitive discriminator. Note that the muon track efficiency is smaller at the higher discriminator levels for tracks near the HV input (where the strip pulse is double-lobed and half-sized) than for tracks far from the HV input.

One of the central requirements in obtaining good muon tracking resolution is to minimize the cross-talk between adjacent strips. The cross-talk has an intrinsic minimum arising from the irreducible coupling between the anode wire and the adjoining strips. Some reduction of cross-talk is possible by tuning the terminating resistor R_T in the HV board circuit as is shown in fig. 11. Measurements were made on a 6 m module triggered by a simple cosmic ray telescope constructed from three 1.5 m modules. Two of the cosmic ray trigger modules were strung with only one wire in them, and the third with all but that wire strung in "logical complement" to the first two. The first two tubes acted to define the muon trajectory and the third was used as a veto. By carefully aligning the telescope over the test chamber, a trajectory could easily be defined within one strip. Figure 15 shows the central hit strip and adjacent strip efficiencies as a function of this resistance for a 1 mV threshold. NIM standard electronics were used for this measurement. We note that there is a broad minimum at about 150 Ω, which is roughly the correct value needed to terminate the transmission line formed by the anode wire and the strip as discussed above. Direct observations of the pulses on the wire corroborated this result.

The electronics used to read out the strips in the final setup is the commercial SGS [15] hybrid discriminator with an adjustable threshold. The electronics have been modified to have a sufficient gain so as to trigger efficiently on proportional mode pulses. Figure 16 shows the efficiency of a chamber for cosmic rays as a function of the HV for two different positions on the chamber. The data were taken with cosmic rays using the "3:1" gas with one discriminator threshold set to 3 mV.

A figure of merit important in describing the muon tracking is the correlation of the chamber efficiency with the average number of strips which trigger the strip readout electronics. Figure 17 shows the average plane efficiency and the average cluster size for muon tracks as a function of the discriminator threshold measured with barrel chambers operating in the SLD detector. The cluster size was defined as the number of contiguous hit strips in a given chamber layer along the muon track. The chambers were filled with the nonflammable three-component gas operated at 4.75 kV. We note that both the efficiency and cluster size decrease as the threshold is increased, but the falloff is slow for the efficiency whereas the cluster size decreases quite rapidly. Operating at a threshold of 3 mV corresponds to a cluster size of three cells and an efficiency of 90%.

We have investigated the dependence of the muon tracking efficiency on the angle of incidence. Data were taken using cosmic rays as a function of Φ, the angle in a plane perpendicular to the wire; and as a function of θ, the angle measured in a plane parallel to the wire. The measured efficiency as a function of Φ averaged over θ is shown in fig. 18. The angle Φ is defined such that $\Phi = 0$ corresponds to a normally incident track. We note that there is a gradual increase in the efficiency from about 90% at small Φ up to almost 100% at $\Phi = 60°$. We attribute this increase in the efficiency as Φ increases to large angle tracks which penetrate multiple cells, thereby diminishing the effective dead space of the U–channel walls.

Figure 19 indicates the efficiency as a function of θ integrated over a range in Φ. The results are consistent with a roughly constant efficiency as expected from geometric considerations. (The probability of a muon track penetrating a cell and not depositing sufficient ionization to initiate a limited streamer is small.) Although the efficiency does not seem to change with this angle, we do notice that the number of multistreamer events increases with increasing θ.

The chamber spatial resolution has been studied using cosmic rays passing through a set of well aligned overlapping chambers. The muon tracks were determined by all of the chambers except the one under study. The cluster center was determined from the digital hit pattern. The results are given in fig. 20. The resolution is $\sigma \approx 0.34$ cm for $\Phi < 45°$, which is only slightly degraded from the intrinsic limit $\sigma \approx 1 \text{ cm}/\sqrt{12} = 0.29$ cm.

5.2. The y–strip readout

The y–strips are 4 cm wide (or 2 cm wide for the endcaps only) electrodes placed perpendicular to the anode wires (and the x–strips) and are used to determine an orthogonal coordinate for the muon tracking. We observe positive-going pulses of a few millivolts amplitude into 50 Ω on the y–strips, which is about the same amplitude as the pulses observed on the x–strips. The same SGS discriminator electronics as employed in the x–strips are used to read out the y–strips.

Of chief concern is the spatial resolution of the y–strip readout. Since the y–strips are perpendicular to the anode wire, they do not form a transmission line in the same manner as the x–strips. As a consequence, the spatial resolution of the y–strips will be different from the x–strips owing to a greater cross-talk. This arises from currents propagating in the cathode plane which couple into adjacent y–strips.

Because of the open profile construction of our limited streamer tubes, we expect a smaller cross-talk to be observed when the y–strips are connected to the top of the profile and are thus at a greater distance from the cathode graphite coating where ground currents flow, than in the case where the y–strips are mounted on the lower side of the profile in proximity to the resistive coating. Figure 21(a) shows the distribution of charge on the y–strips normalized to the central strip for y–strips mounted on the open side of the profile. The figure clearly indicates that in the case of the y–strips mounted on the open side, there is a narrower distribution than in the bottom case, shown in fig. 21(b). Such a high cluster multiplicity would degrade the track resolution considerably. For comparison, we show in fig. 21(c) the corresponding distribution for x–strips which we see is even narrower than the top-mounted configuration shown in fig. 21(a).

The correlation of the y–strip efficiency with the y–strip multiplicity for the two configurations is shown in fig. 22. We note that for the top mounted configuration we can achieve a reasonable efficiency ($\approx$ 90%) with a small cluster size ($\approx$ 2 y–strips full width), whereas for the bottom mounted configuration, the requirement of a small cluster size significantly reduces the layer efficiency. Therefore, we have chosen to mount the

y–strips on the open side of the profile. Our results are in qualitative agreement with those of the UA1 Collaboration [16].

5.3. The pad readout

The total charge accumulated on the pad towers determines the energy deposited in the iron calorimeter [17]. Typical pad sizes are 20 cm $\times$ 20 cm with a capacitance to ground of about 2 nF, but both the size and capacitance vary widely from these average values as dictated by the projective geometry. The construction of the chambers is such that a typical pad covers several modules on a chamber, as well as several pads overlapping a given module. The endcap chambers were constructed with a double PVC plastic sleeve which enables bad modules to be replaced without delaminating the entire chamber. The double sleeve, however, tends to diminish the measured charge on the pads by about 10%. This effect will be taken into account in the energy calibration of the calorimeter.

As we have noted, the pad pulses are positive-going and the charge collected on them is roughly one-half of the absolute magnitude of the charge on the wire. This is consistent with the geometric construction wherein the pads subtend roughly one-half of the total solid angle from a streamer. The pads are read out by a hybridized charge-sensitive amplifier [18] and a LSI sample-and-hold device [19].

The tower structure of the pad readout allows the energy deposition in separate jets to be resolved, which is of interest in QCD and other studies. To understand how the separate pad tower calorimetry will work, we have measured the cross-talk between the pads by means of cosmic ray muons and a ^{90}Sr source. The pad cross-talk is not as critical as in the case of the x– or y–strips, where the cross-talk directly degrades the muon track resolution. The cross-talk in the pad system should not strongly affect the total energy measurement but may influence the hadron jet definition. In fig. 23 we compare the pulses on a central pad with the pulses on a pad which is adjacent along the modules [fig. 23(a)], and on a pad which is adjacent in the direction perpendicular to the modules [fig. 23(b)]. We note that the cross-talk on the pads mounted on adjacent modules tends to be smaller than those on pads sharing the same modules.

Given the typical "ringing" time structure of the pulses shown in fig. 23, the magnitude of the integrated cross-talk will depend on the integration time. We have used our hybrid integrator, which has an integration time of 5 μsec, to measure the pad-to-pad cross-talk on a test chamber. Both cosmic rays and a ^{90}Sr source centered on a given pad were used to obtain the data. The results are shown in fig. 24, where we note that the adjacent pad along the module has a cross-talk of about 10%. Further away along the same module from the central pad, the cross-talk decreases with increasing distance from the central pad. The pad cross-talk is observed to go negative to about −2% for pads which are four to five towers away from the central tower. This behavior is assumed to arise from the irreducible coupling of the pulse propagating down the wire and the resistive cathode to the other pads. The same pattern is observed on the y–strips. In contrast to the cross-talk observed in pads which share the same module, the cross-talk on adjacent pads which do not have any modules in common was found to be essentially zero.

6. Operating characteristics

Reliable operation of the WIC calorimetry and muon tracking rests on maintaining the stability of the chamber response under changes in HV, gas mixture, discriminator threshold, and various ambient conditions. In this section, we discuss the choice of the operating point and its sensitivity to various parameters.

6.1. *Choice of the operating point*

A primary consideration in fixing the operating point of the chambers is the choice of the gas. Since the limited streamer chambers will be operated in a confined space near HV and high currents, it was imperative to have a nonflammable gas mixture. After considerable effort [11] we developed the nonflammable three-component gas, and have demonstrated that it has acceptable characteristics in terms of chamber operation as well as being nonflammable. Our chosen operating point with this safe gas is at 4.75 kV with 100 μm wires. Some small adjustments of this voltage may be necessary in the operating detector since no attempt will be made to control the temperature and pressure of the gas inside the tubes.

We have chosen the HV operating point to be well above the transition between the proportional mode and the limited streamer mode, yet below the point where significant multistreamer production takes place. Referring to fig. 7, we note that once the limited streamer threshold has been reached, the fraction of proportional mode rapidly decreases with increasing HV for any gas mixture. Our criterion is to fix the operating point to be above the voltage at which the proportional mode is less than 5% of the limited streamer mode. For example, for the 3:1 gas mixture, this point is 4.65 kV, and for the safe nonflammable three-component gas it is 4.75 kV.

6.2. *Sensitivity to the HV*

The charge integrated on the energy-measuring pad towers depends on the HV through the variation of the charge per pulse shown in fig. 5. We find that on the anode wire $dQ\ (\text{wire})/dV \approx 60$ pC/kV so the pad response is about $dQ\ (\text{pad})/dV \approx 30$ pC/kV. If we operate at a point where a single minimum ionizing track through one pad gives

16 pC on the pad, then to maintain the stability of this point to 1% we require the HV to be stable to within 5 V, or 0.1% of its value. The commercial CAEN HV power supply [20] meets this specification.

The efficiency of the x– and y–strip readout may also depend on the HV. As the HV is changed, the streamer mode pulse amplitude and the fraction of pulses in the limited streamer mode will change. This results in a loss of efficiency if the discriminator threshold is too high. Figure 25 shows the efficiency of the strip readout as a function of the discriminator threshold for several HV values. The data indicate that for HV values above 4.8 kV, the strip readout efficiency is nearly independent of the threshold value for thresholds up to about 8 mV.

6.3. *Sensitivity to ambient temperature and pressure*

The limited streamer mechanism depends on gas density in the usual manner, namely: the greater the density, the shorter the electron mean-free–path and the smaller the energy gain between collisions, resulting in less secondary ionization per unit length. Therefore the greater the gas density, the smaller the gas gain. The effect of temperature changes at constant pressure on the average pad charge is shown in fig. 26. The slope dQ/dT both for the 3:1 gas and the nonflammable three-component gas appears to be the same. We find that the operating point dependence on the temperature is:

$$\frac{dQ}{Q} = K_T \frac{dT}{T} \quad , \tag{3}$$

where T is the absolute temperature, and $K_T = 10.4 \pm 0.5$ for the 3:1 gas and 7.5 ± 0.5 for the three-component gas. K_T is smaller for the three-component gas because dQ/dT is the same for both, but Q is larger. Data were also taken on the pad gain at constant temperature as a function of ambient pressure. The result was, for the 3:1 gas at 4.65 kV:

$$\frac{dQ}{Q} = -(9.1 \pm 1.0)\,\frac{dP}{P} \quad , \tag{4}$$

which is consistent with the values of K_T given above.

It is important to remember that the change in gas gain due to change in the density not only modifies the streamer gain, but also displaces the location of the proportional-streamer transition. Since the operating point is chosen to be at the point where the proportional mode is less than 5% of the streamer mode, a reduction in the gas gain tends to decrease the streamer fraction making the effective gain change more pronounced. Therefore, we plan to monitor the ambient temperature, pressure, and gas gain quite carefully during data taking. Small adjustments in the HV may have to be made to maintain the desired operating point.

6.4. *Sensitivity to the gas mixture*

We have studied the sensitivity of the tube performance to small changes in the gas mixture. For our nonflammable three-component gas mixture we find that the gain is directly proportional to the argon content, namely $dQ/Q = dA/A$, where A is the argon fraction. A similar result is obtained for variations in the isobutane content. We believe that the operating point will be easy to maintain given the accuracy of the mass flow controllers which regulate the gas mixture.

It is interesting to note that the results with 3:1 gas [isobutane (75%)–argon (25%)] seem to be more sensitive to variations in the gas mixture. For example, changing the isobutane–argon mixture to 74%–26% (76%–24%) changes the gain as measured in the mean pad charge by 19% (−18%). Expressed in terms of the argon content, the gas mixture sensitivity for this binary mixture is: $dQ/Q = 4.5\ dA/A$.

6.5. Sensitivity to gas purity

The gas purity is another parameter which affects detector performance. The most expensive component of the gas mixture is the isobutane which would be quite costly if purchased in a highly purified form. Fortunately, the impurities found in the inexpensive grades of this gas do not strongly affect the operation of the chambers. In the bulk grade isobutane, the chief impurities are propane (typically 1.4%) and normal butane ($\approx 0.7\%$). We compared the limited streamer gain using 99% pure isobutane versus the bulk-grade isobutane and found a 50 V shift in the operating point which could be corrected by raising the HV. All of the measurements quoted above were taken with the bulk grade gas.

Another impurity is water which diffuses through the plastic covers from the surrounding air. The chambers have such a large surface area that appreciable water diffusion is impossible to eliminate. By using a gas chromatograph we found that the water fraction inside the chambers follows the absolute humidity outside. This correlation is shown in fig. 27. At equilibrium, the water concentration inside the chambers is given by:

$$N(t_0) \;=\; N_0 \, \frac{\alpha}{(\alpha + 1/t_0)} \quad , \tag{5}$$

where t_0 is the time for one volume change, N_0 is the water concentration outside, and the permeation coefficient for PVC plastic $\alpha = 5.5 \times 10^{-5}$ sec^{-1}. In humid conditions, when the gas volume of the chambers is changed slowly (on the order of once per day), the water content inside the chambers can reach as much as 1.0% by gas volume. This quantity of water does not seem to affect the operating characteristics of the chamber.

The PVC plastic from which the chambers are constructed may outgas and contaminate the gas, thereby affecting the operation of the chambers. If this process were to occur, we would expect that the operating point would change as the gas flow is changed. Therefore, we measured the efficiency and gas gain for several gas flows from one volume change every few hours down to one volume change every 48 hours. Throughout this range no change in the operating characteristics was observed.

6.6. Radiation damage studies

Although we expect that the radiation exposure will be small in our particular application of the limited streamer tubes, other experiments at hadron machines may be subjected to higher levels. Therefore, it is interesting to measure the damage which may occur to a limited streamer tube when it is exposed to intense local radiation.

Radiation damage was induced by a 16 μC ^{106}Ru β–source (3.5 MeV endpoint energy). The radiation dosage was measured by the change of the mean collected charge per-pulse on the anode wire as a function of accumulated charge. To insure that the measurement was not influenced by various instabilities, the mean height of the charge spectrum in the damage region was normalized to the charge spectra in two fiducial regions laterally displaced from the "hot" spot. A lateral displacement was chosen for the fiducial regions since the damage may propagate down the wire by photoionization. The radiation damage spot was located in the center of a 6 m extrusion. The tube was operated in the limited streamer mode at 4.65 kV using the 3:1 gas mixture. The chamber gas also contained water at roughly 1% by volume by diffusion from outside humid air.

The ^{106}Ru source was placed directly on the copper cladding ground shield of the limited streamer tube thereby limiting the β–radiation to an area of roughly 1 cm^2. Under this condition the current drawn by the tube was $\langle i \rangle \approx 2.5$ μA with a corresponding counting rate of 12 kHz for pulses on the anode wire above a discriminator threshold of 3.8 mV. Therefore, a total charge of roughly 0.22 C was accumulated per day (as measured by integrating the current load on the power supply). The background current when the source was removed was $\langle i \rangle \approx 0.06\ \mu$A. The data of the charge spectrum were taken with the source collimated to one cell at a current of $\langle i \rangle \approx 1.2\ \mu$A and counting rate of 6.2 kHz.

The results are shown in fig. 28. We note that the peak of the charge spectrum decreases by about 13% for the first Coulomb of accumulated charge, but thereafter remains roughly constant out to about 4 C. The water content in the chamber gas may have decreased the rate of the radiation damage [21]. We expect that the conditions under which the tubes will operate in the SLD detector will correspond to several orders of magnitude less radiation dosage than this test. Hence we do not anticipate that radiation damage will be a problem.

6.7. *Life test of the modules*

We plan to operate the limited streamer chambers of the SLD for several years as we accumulate statistics on e^+e^- collisions in the Z^0 mass range. This physics goal makes stringent demands on the reliability of the modules. Our detector is built so that it is possible to replace a bad module in the endcap chambers, but a nonworking module in the barrel region can not be replaced simply. We therefore require that the failure rate of the modules be less than about 2% per year, thereby limiting the cumulative failure to 10% over the five-year duration of the experiment. To verify that our construction techniques and choice of operating point satisfy this criterion, we performed a life test of the modules.

The life test was performed in two phases. In the first phase, we operated roughly 1066 modules (6 m long) with the 3:1 gas mixture. Half of these modules were maintained at 4.65 kV in the limited streamer mode, and half were operated at 4.1 kV in the proportional mode. In the second phase about 400 modules were filled with our nonflammable three-component gas and operated at 4.75 kV. In both phases of the test the HV was turned off every 12 hours for a few minutes. All of the modules in both phases of the test passed the standard conditioning and acceptance tests performed on the production modules of the installed chambers [3].

A module was defined to fail the life test when it drew a steady current of 200 μA (the fixed current limit of the CAEN HV power supply), or a current greater than 20 μA for more than 10% of the time. In the first phase using the 3:1 gas we accumulated 45,858 module-days in the limited streamer mode and 33,116 module-days in the proportional mode. In the second phase 44,675 module-days were accumulated with our nonflammable three-component gas. One failure in the limited streamer mode was found in several months of operation, but was associated with a displaced wire—a construction defect. One failure in the proportional mode was detected of unknown causes. (We opened this module but found no cause for it to fail.) The combined failure rate of the modules operated in the limited streamer mode is $< 1.9\%/\mathrm{yr}$ at the 90% confidence level for each gas mixture assuming the failure rate is constant. We conclude that the modules will have a sufficient longevity to perform the experiment.

7. Conclusions

We have constructed a large calorimeter and muon tracking device based on limited streamer tubes for the SLD experiment at SLAC. Our various tests of the operating characteristics indicate that the device is robust and comparatively simple to use. We have gained an understanding of the limited streamer mechanism, studied the x– and y–strip readout, measured the tracking efficiencies under various changes of parameters, and explored the cross-talk in both the strip and the pad readouts. The stability of the operating point was studied as a function of the gas density, radiation exposure, and operating-time.

Acknowledgments

The successful design and construction of this detector system could not have been accomplished without the help of a large number of skilled people. Particular thanks are due to F. Babucci, G. Bonora, U. Cazzola, E. Druek, D. Ross, and D. Sawyer for their dedicated efforts and contributions. The authors would also like to acknowledge the able technical assistance of the following: V. Giordano and A. Zucchini (Bologna); S. Bigoni, V. D'Orto, and C. Fordiani (Ferrara); D. Pistoni (Frascati); the Campana Crew (MIT); G. Marinolli, B. Migliorato, and A. Paonessa (Padova); E. Babucci and G. Chiocci (Perugia); F. Bosi, L. Corucci, G. Gausto, and L. Zaccarelli (Pisa); and N. Erickson, J. Escalera, M. Mittmann, R. Parsons, P. Ritson, and crews at IR–6 and the Light Assembly Building (SLAC). In addition, we would like to express our appreciation for the extensive use of the routing machinery at the Fermi National Accelerator Laboratory.

References

[1] SLD Design Report, SLAC–Report 273 (1984);

M. Breidenbach, IEEE Trans. Nucl. Sci. **NS–39** (1986) 46.

[2] S. Brehin *et al.,* Nucl. Instr. and Meth. **123** (1975) 225;

E. Iarocci, Nucl. Instr. and Meth. **A217** (1983) 30;

G. Battistoni *et al.,* ibid., 429;

G. Battistoni *et al.,* Nucl. Instr. and Meth. **A245** (1986) 277;

W. Busza, Nucl. Instr. and Meth. **A265** (1988) 210.

[3] A. C. Benvenuti *et al.,* Nucl. Instr. and Meth. **A276** (1989) 94.

[4] L. S. Osborne, Proc. on Gas Sampling Calorimetry Workshop II, Fermilab (1985), eds. M. Atac, G. Brandenberg, M. Mishina.

[5] M. Atac *et al.,* Nucl. Instr. and Meth. **200** (1982) 345.

[6] The mass-flow controller was manufactured by Datametrics, Dresser Industries, Wilmington, MA 01887, USA.

[7] The gas chromatograph was made by Gow–Mac Instrument Co., Bridgewater, NJ, USA.

[8] LeCroy Corporation, 700 Chestnut Ridge, Chestnut Ridge, NY, USA.

[9] F. Sauli, CERN 77–09 (1977).

[10] H. Raether, *Electron Avalanches and Breakdown in Gases,* Butterworths Publishers, London (1964); F. E. Taylor, submitted to Nucl. Instr. and Meth. (1989).

[11] S. Cartwright *et al.,* SLAC–SLD–NOTE 185 (1988);

R. Battiston, Third Topical Conf. on Perspectives for Experimental Apparatus at Future High Energy Machines and Underground Laboratories, San Miniato, Italy (1988); Nucl. Instr. and Meth. **A277** (1989) 279;

A. C. Benvenuti *et al.,* SLAC–PUB–4687 (1989).

[12] R. W. Zdarko *et al.,* Proc. of the APS/DPF Meeting, Salt Lake City, Utah (1987);

G. Callegari *et al.,* SLAC–PUB–4461 (1987).

[13] G. Battistoni *et al.,* Nucl. Instr. and Meth. **202** (1982) 459.

[14] F. Kajino *et al.,* Nucl. Instr. and Meth. **A245** (1986) 507.

[15] F. Beconcini *et al.,* INFN/TC–86/17 (1986).

[16] A. Bettini *et al.,* UA1–TN 84–10 (1984).

[17] Preliminary prototype studies of a test calorimeter were reported in G. Callegari *et al.,* IEEE Trans. Nucl. Sci. **NS–33** (1986) 201.

[18] B. Wadsworth *et al.,* in preparation.

[19] G. M. Haller *et al.,* IEEE Trans. Nucl. Sci. **NS–33** (1986) 221.

[20] SY127 High Voltage System, CAEN, Viareggio, Italy.

[21] J. P. DeWulf *et al.,* Nucl. Instr. and Meth. **A263** (1988) 109;

R. Kotthaus, Nucl. Instr. and Meth. **A252** (1986) 531;

J. P. Venuti and G. B. Chadwick, IEEE Trans. Nucl. Sci. **NS–36** (1989) 595.

Figure Captions

Fig. 1. (a) Overview of the instrumented iron structure of the SLD, called "WIC" for "Warm Iron Calorimeter." Shown are the barrel section covering the polar angles from about 45° to 135° and the endcaps. The 45° chambers which cover the overlap region between the barrel and endcaps are not shown. The barrel and endcap chambers perform both muon tracking and calorimetry functions, while the 45° chambers are used only for muon tracking.

(b) Cross sectional view of the barrel and endcap installations.The limited streamer tubes are mounted between the 5-cm-thick iron plates. The projective geometry of the pad towers is indicated.

Fig. 2. Cutaway view of a module. Shown is the U-shaped PVC channel coated with graphite. The eight wires are connected to the resistor card at the end of the module. The plastic piece at the end of the module contains the gas and HV connections. Bridges support the wire in the graphite coated profiles every 40 cm.

Fig. 3. Typical pulses on the anode wire into 50 Ω from streamers far from (a), midway (b), and near (c) the HV input of a 6 m tube. Note that the pulses from streamers far from the HV input are single-lobed, whereas those from streamers near the HV input are double-lobed from the reflection at the unterminated end of the tube. The pulses were photographed with the chamber operated at 4.8 kV using the 3:1 isobutane–argon gas mixture.

Fig. 4. Exploded view of the endcap chamber construction indicating the modules, strips, pads, and shielding ground planes. The stripline mounted above the pads is used to read out the pads. In the barrel chambers, a flat cable, instead of a stripline, is used. Not shown is the double-sleeve construction of the chambers.

Fig. 5. The peak value of the integrated charge on the wire as a function of HV for a 50 μm and a 100 μm wire. A LeCroy QVT was used with a 500 ns gate. Both wires operate in the proportional mode for low HV and show a sudden transition to the limited streamer mode as the HV is increased. The proportional mode is characterized by an exponential dependence on the HV and the limited streamer mode by a linear HV response.

Fig. 6. Pulse height spectra as a function of high voltage and isobutane concentration in argon–isobutane mixtures. The HV ranges from 3600–4800 V and the fraction of isobutane ranges from 60%–80%. The data were taken with cosmic rays on test chambers of the barrel-style construction.

Fig. 7. Shown versus high voltage, for various concentrations of isobutane in argon are: (a) the peak of the streamer pulse height distribution, (b) the peak of the proportional mode pulse height distribution, and (c) the percentage of the pulses judged to be in the streamer mode. For the 75% and 80% isobutane curves in Fig. 7(c), the two modes were indistinguishable at the upper end of the voltage scale and the data are consistent with 100% streamer mode.

Fig. 8. The charge on the wire versus the sum of the charge on all the strips plus the charge on all the pads. Note that there is a good correlation between these charges as expected from electrostatics.

Fig. 9. A scatter plot showing the charge on the pads versus the summed charge on the strips for two argon–isobutane gas mixtures at two different voltages. The corresponding summed pad pulse height, measured in arbitrary units ("sham counts"), is also shown. In (a) the gas was argon (25%)–isobutane (75%) at 4.65 kV, and in (b) argon (35%)–isobutane (65%) at 4.1 kV. The proportional mode, corresponding to

small pulse heights in both the strips and the pads, has a tighter correlation than the larger pulse heights of the limited streamer mode, where the streamers are longer and the geometric fluctuations are larger. The data were taken with a 100 μm wire.

Fig. 10. The correlation of the summed pad pulse height versus that of the summed strips for the nonflammable three-component gas operated at 4.75 kV. The pulse heights are given in arbitrary units.

Fig. 11. The HV circuit is shown. The elements enclosed within the dotted line are mounted on the HV board itself. The HV from the board is connected to the modules by < 1 m of unshielded HV insulated cable. The resistor R_T was tuned to minimize the strip-to-strip cross-talk. Pulses can be injected at the point "P" to test the readout electronics.

Fig. 12. A simplified equivalent circuit for the x–strip readout showing the transmission lines. The first transmission line is formed by the anode wire and the strip and has a characteristic impedance of about 400 Ω. The high resistance cathode plane is indicated by the dotted lines. The cathode plane is considered to be transparent for fast transients. The other transmission line is a strip line formed between the strip and the ground shield with an impedance of 33 Ω. The signal is measured between the strip line and the ground.

Fig. 13. The strip pulse is compared with the pulse on the wire for two positions along the wire: (a) far from, and (b) near the HV connection. Note that when the pulse on the wire is double-lobed, so is the pulse on the strip in agreement with our transmission line model.

Fig. 14. The dependence of the strip efficiency on the position from the HV input for various voltage-sensitive discriminator levels is shown. For the higher discriminator levels, the efficiency is less when the streamer is close to the HV input than when it is far away.

Fig. 15. The dependence of strip cross-talk on the resistor R_T of the HV board is shown for a 1 mV discriminator threshold. The central strip was at position number four. The strip-to-strip cross-talk is minimized by setting $R_T = 150\ \Omega$. Note that this value is close to that needed to terminate the wire-strip transmission line.

Fig. 16. The strip efficiency of the chamber as a function of HV at two positions along the module: near the HV input (open circle), and far from the HV input (closed circle). The electronics threshold was fixed at 3 mV.

Fig. 17. The average x–strip efficiency (closed circles) and cluster size (open circles) for cosmic rays plotted as functions of the voltage threshold of the SGS discriminator. The data were taken with our preliminary setup using actual chambers installed in the barrel region of the SLD operated at 4.75 kV with our safe gas. The figure indicates that $V_{threshold} > 3$ mV is needed to obtain a multiplicity of < 3 hit strips. However, at this threshold the layer efficiency is $\approx 90\%$.

Fig. 18. The x–strip efficiency as a function of Φ, the angle measured in a plane perpendicular to the wire with $\Phi = 0$ for normal incidence. For small Φ, the muon track penetrates only one cell, but as Φ increases more than one cell is traversed thereby reducing the effect of the dead space in the U–channel walls of the PVC profile.

Fig. 19. The x–strip efficiency as a function of θ, the angle in the plane parallel to the wire, with $\theta = 0$ for normal incidence. The results are consistent with the geometric limits.

Fig. 20. The muon track spatial resolution normalized to the intrinsic resolution of 1 cm/$\sqrt{12}$ as a function of the angle Φ for the digital cluster center-finding algorithm. The resolution is close to the intrinsic limit given the size of the x–strips. The spatial resolution is not strongly dependent on the angle Φ for $\Phi \lesssim 30°$.

Fig. 21. The distribution of induced charge collected on the y–strips, normalized to the central strip. Data from the two mounting configurations are shown: (a) the y–strips are mounted on the top of the profile, (b) the y–strips are mounted on the bottom of the profile, and (c) the corresponding charge distribution for the x–strips. We note that x–strip distribution is the narrowest of the distributions and that there is a dramatic difference between the two mounting configurations for the y–strips.

Fig. 22. The correlation of the y–strip efficiency with the y–strip multiplicity is shown for the two mounting configurations (a) top of the profile, (b) bottom of the profile. Note that the top mounted configuration is preferred. A rough conversion of the threshold scale is 100 units, corresponding to 2.22 mV.

Fig. 23. The pulses on the central pad [upper traces (a) and (b)] and adjacent pads into 50 Ω. Note that the pads which are adjacent along the module [lower trace (a)] have a larger cross-talk than those adjacent but not sharing a module [lower trace (b)].

Fig. 24. The pad-to-pad cross-talk as measured by the hybridized charge amplifier with an integration time constant of 5 μsec. The central pad was roughly in the center of the 6 m chamber. The other pads shared the same module and extended nearly to the outer edge of the chamber.

Fig. 25. The x–strip efficiency for cosmic rays at various fixed HV values as a function of the discriminator setting. The data were taken with our three-component non-flammable gas at a distance of about 2 m from the strip readout end of the module.

Fig. 26. The integrated pad charge for cosmic rays is plotted versus the ambient temperature at constant pressure for two different gas mixtures. We note that the slopes dQ/dT are the same.

Fig. 27. The water in a limited streamer chamber measured as a fraction (in %) by volume is plotted against the relative humidity at 20°C. The gas volume was changed every nine hours. Note that the chamber water tracks the relative humidity quite well indicating that the PVC plastic is quite permeable to water. The absolute calibration of the water content is accurate to only 30%.

Fig. 28. The mean charge per pulse collected on the wire as a function of the accumulated radiation measured in Coulombs integrated on the anode wire. We note that the radiation damage takes place primarily in the first Coulomb of the exposure.

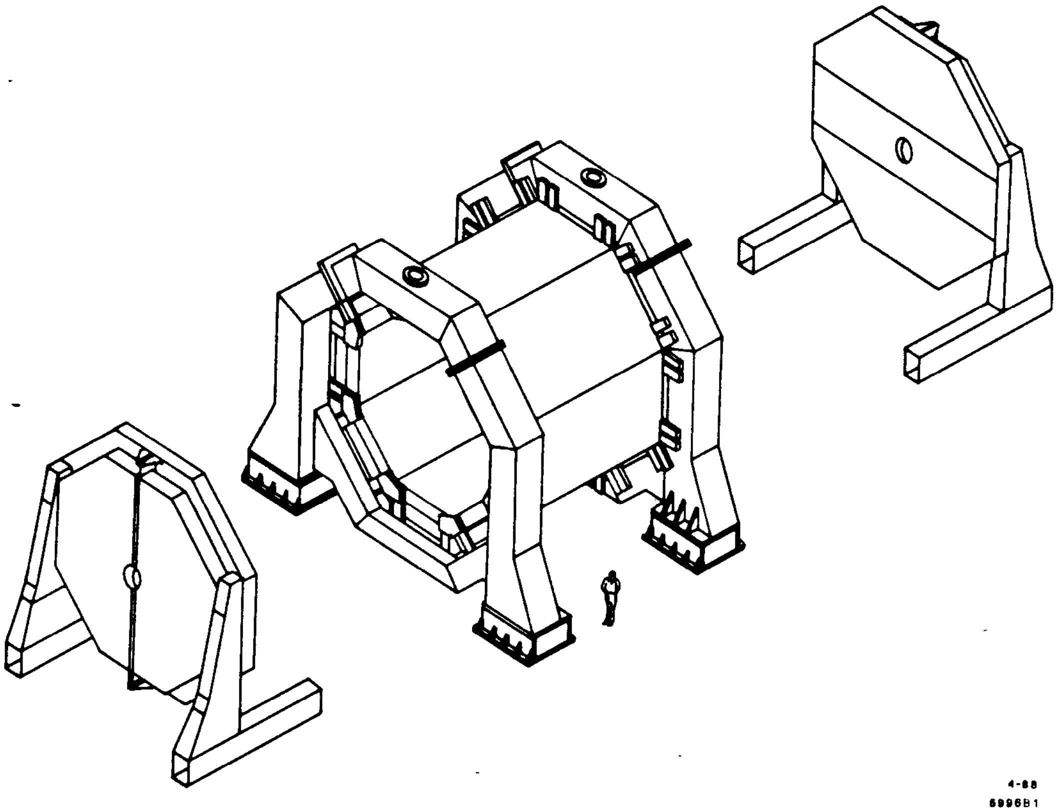

Fig. 1a

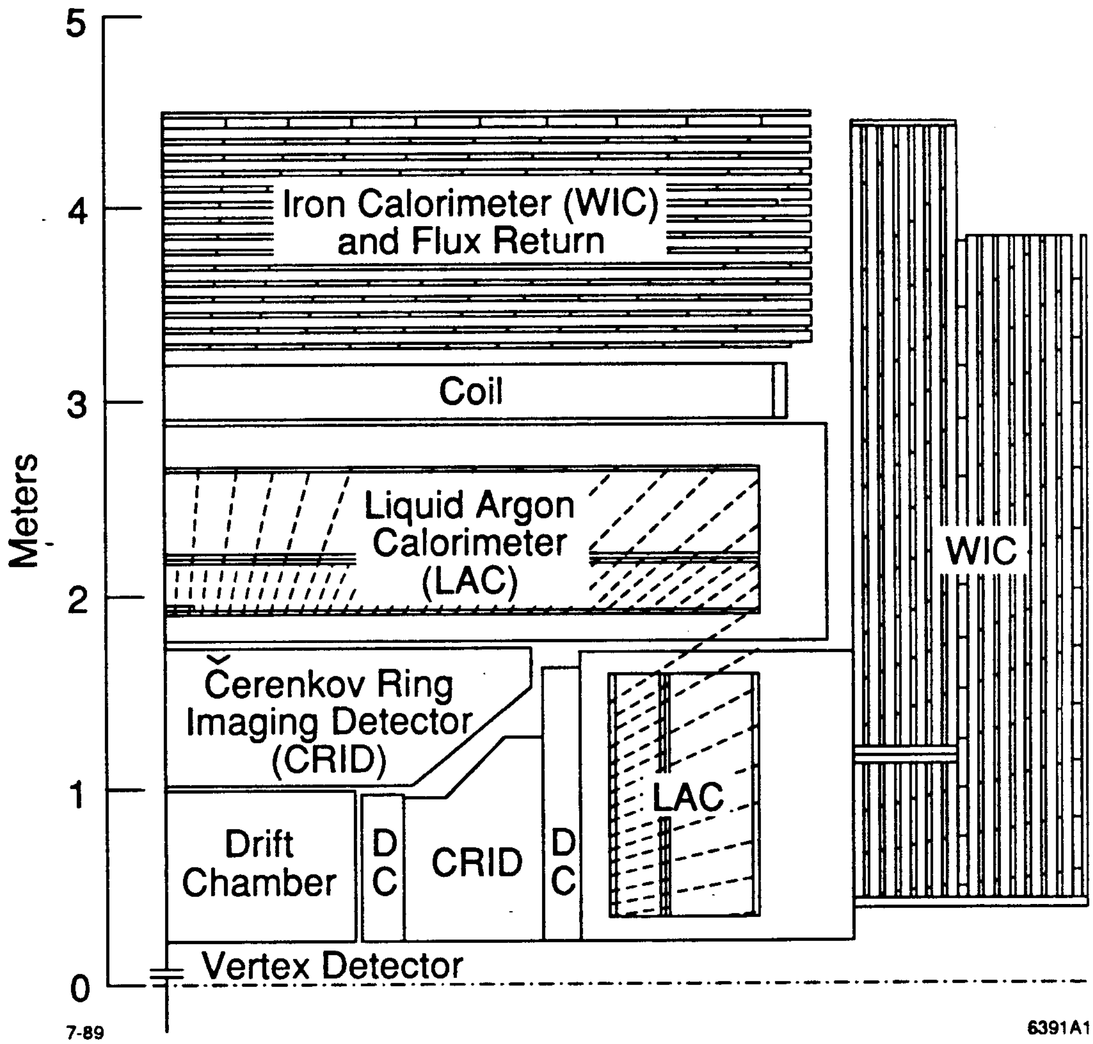
5
4
3
2
1
0
Meters
Iron Calorimeter (WIC) and Flux Return
Coil
Liquid Argon Calorimeter (LAC)
Čerenkov Ring Imaging Detector (CRID)
Drift Chamber
DC
CRID
DC
LAC
WIC
Vertex Detector
7-89
6391A1

Fig. 1b

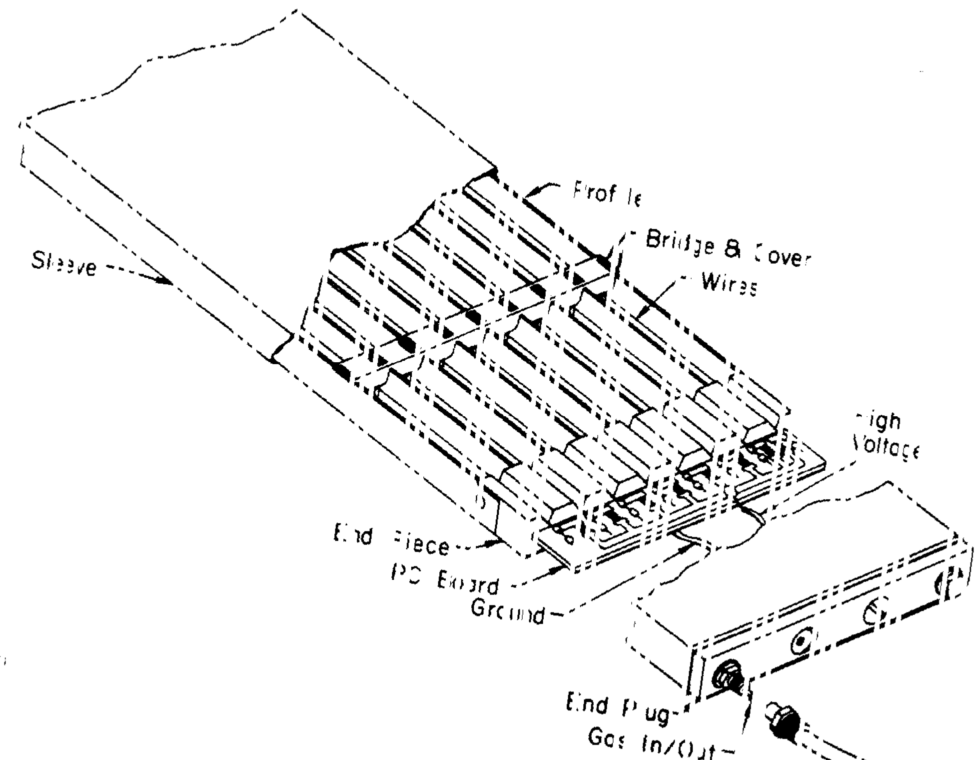
Profile
Bridge & Cover
Wires
Sleeve
High Voltage
End Piece
PC Board
Ground
End Plug
Gas In/Out

Fig. 2

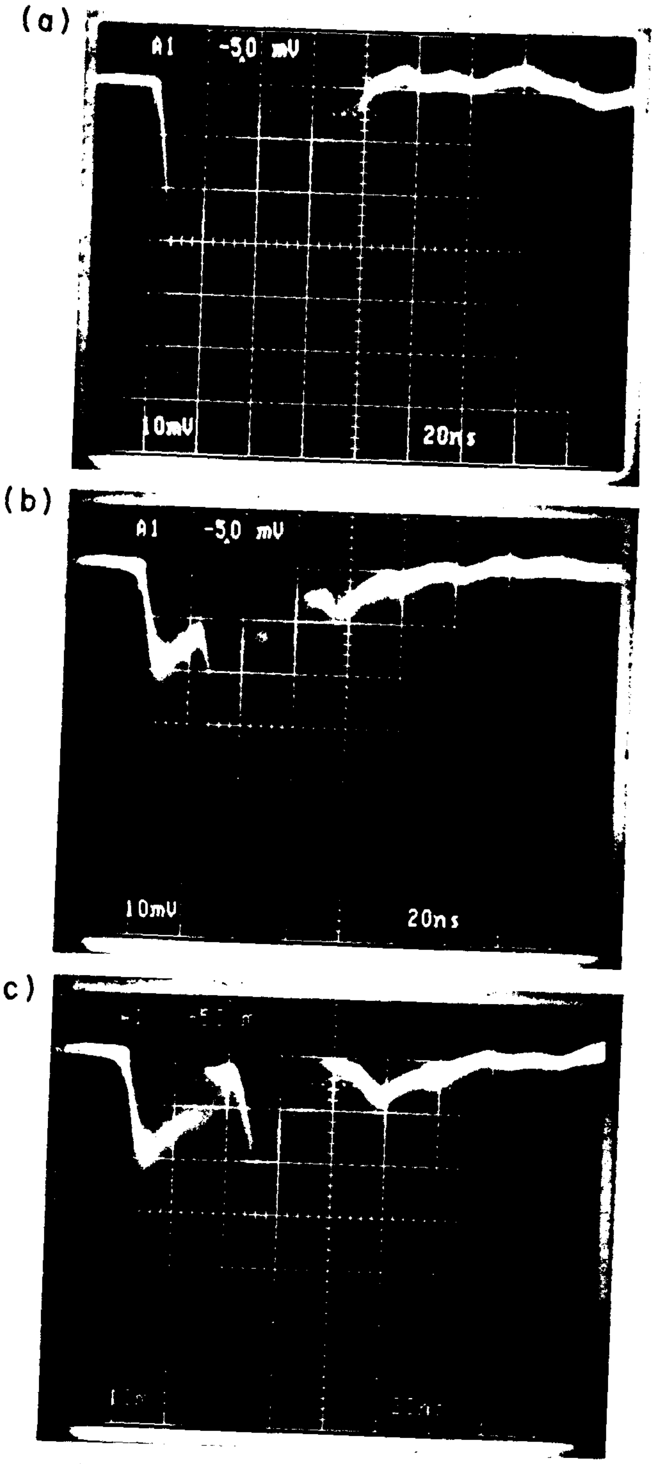

6-89

6363A11

Fig. 3

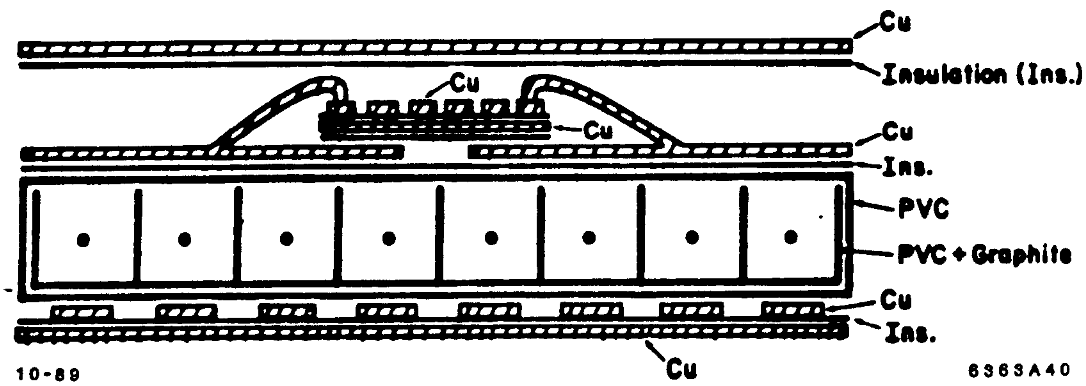
Cu
Insulation (Ins.)
Cu
Cu
Cu
Ins.
PVC
PVC + Graphite
Cu
Ins.
Cu
10-89
6363A40

Fig. 4

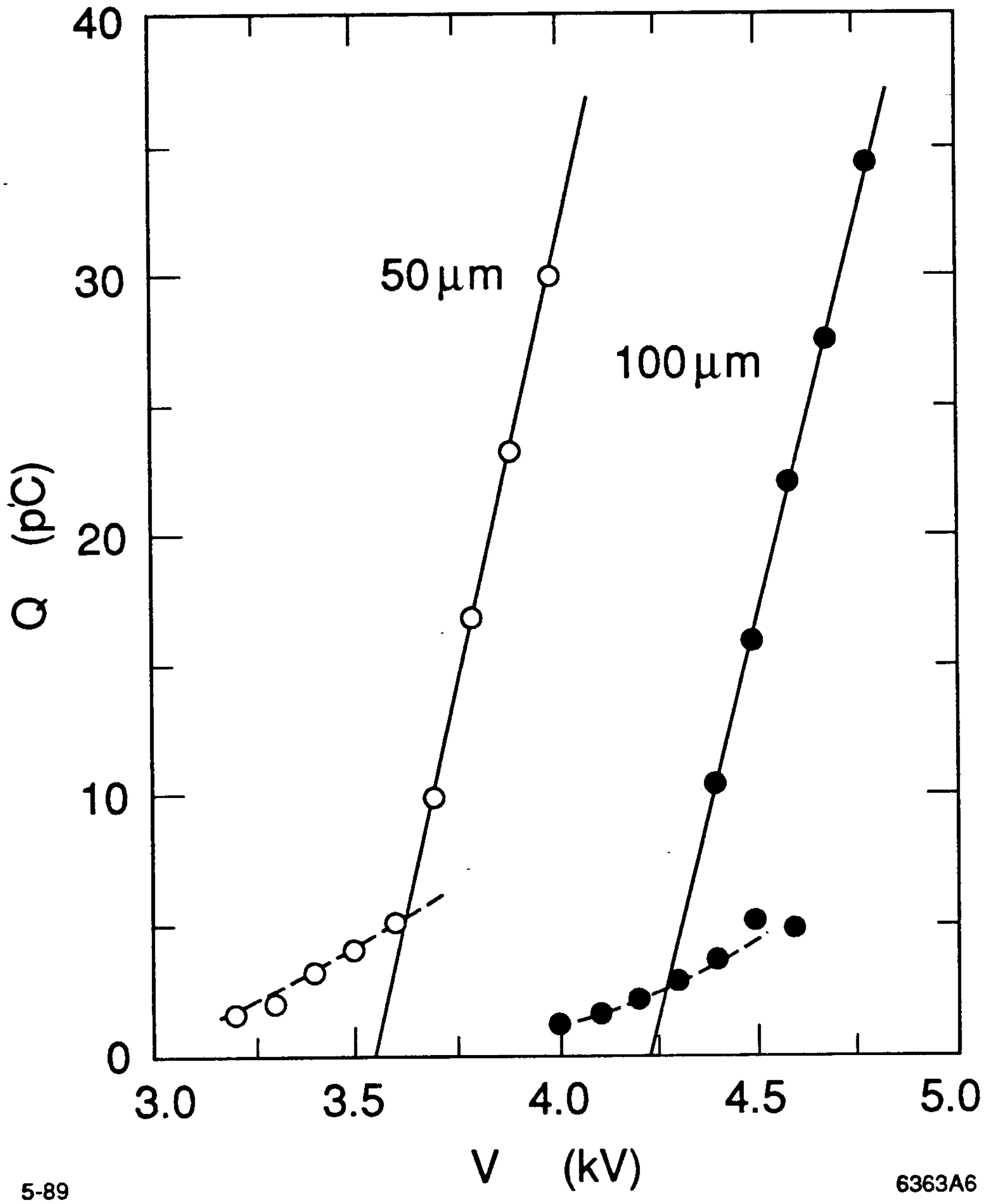

Fig. 5

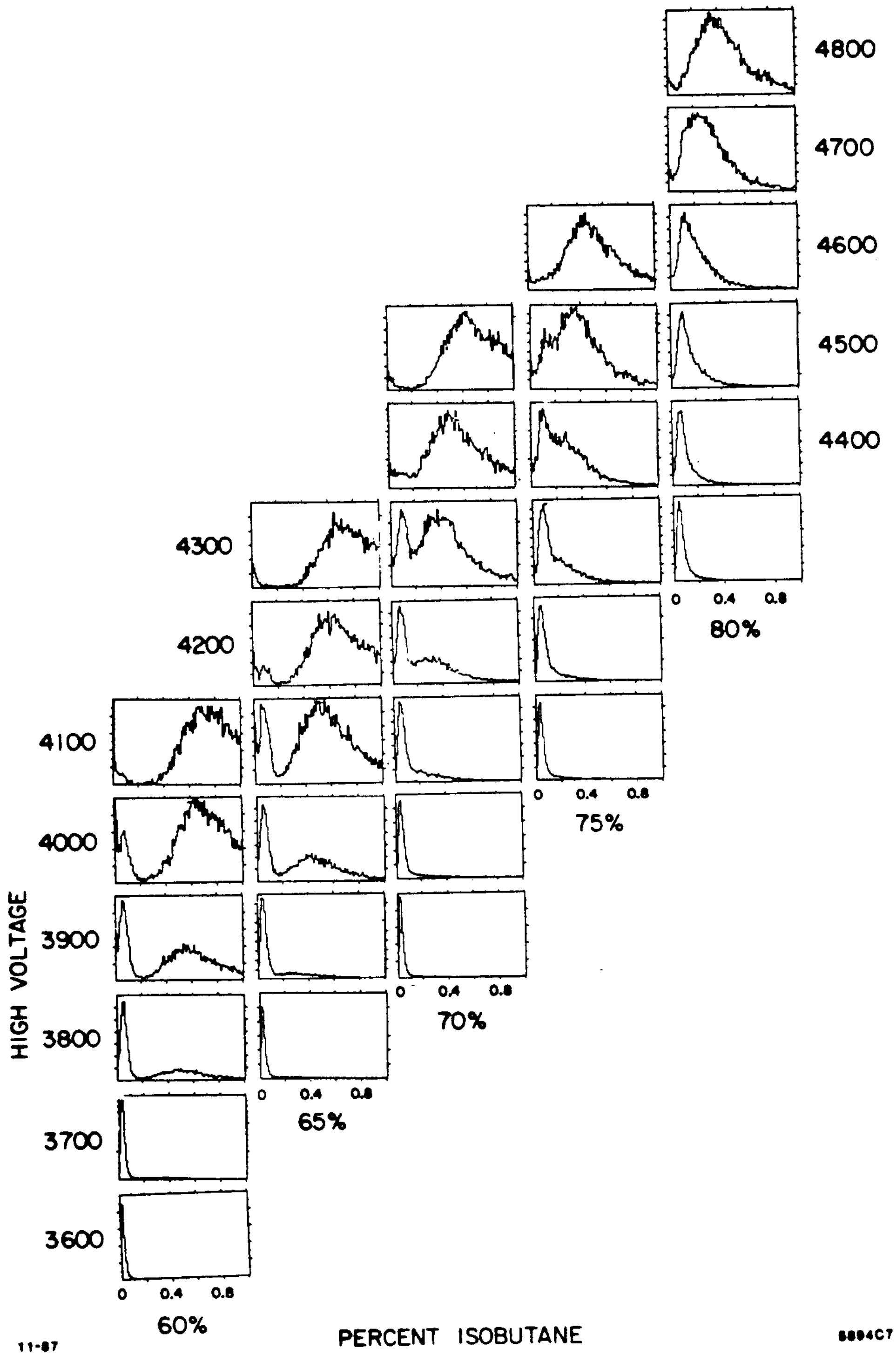
4800
4700
4600
4500
4400
4300
4200
4100
4000
3900
3800
3700
3600
HIGH VOLTAGE
0 0.4 0.8
60%
65%
70%
75%
80%
PERCENT ISOBUTANE
11-87
5894C7

Fig 6

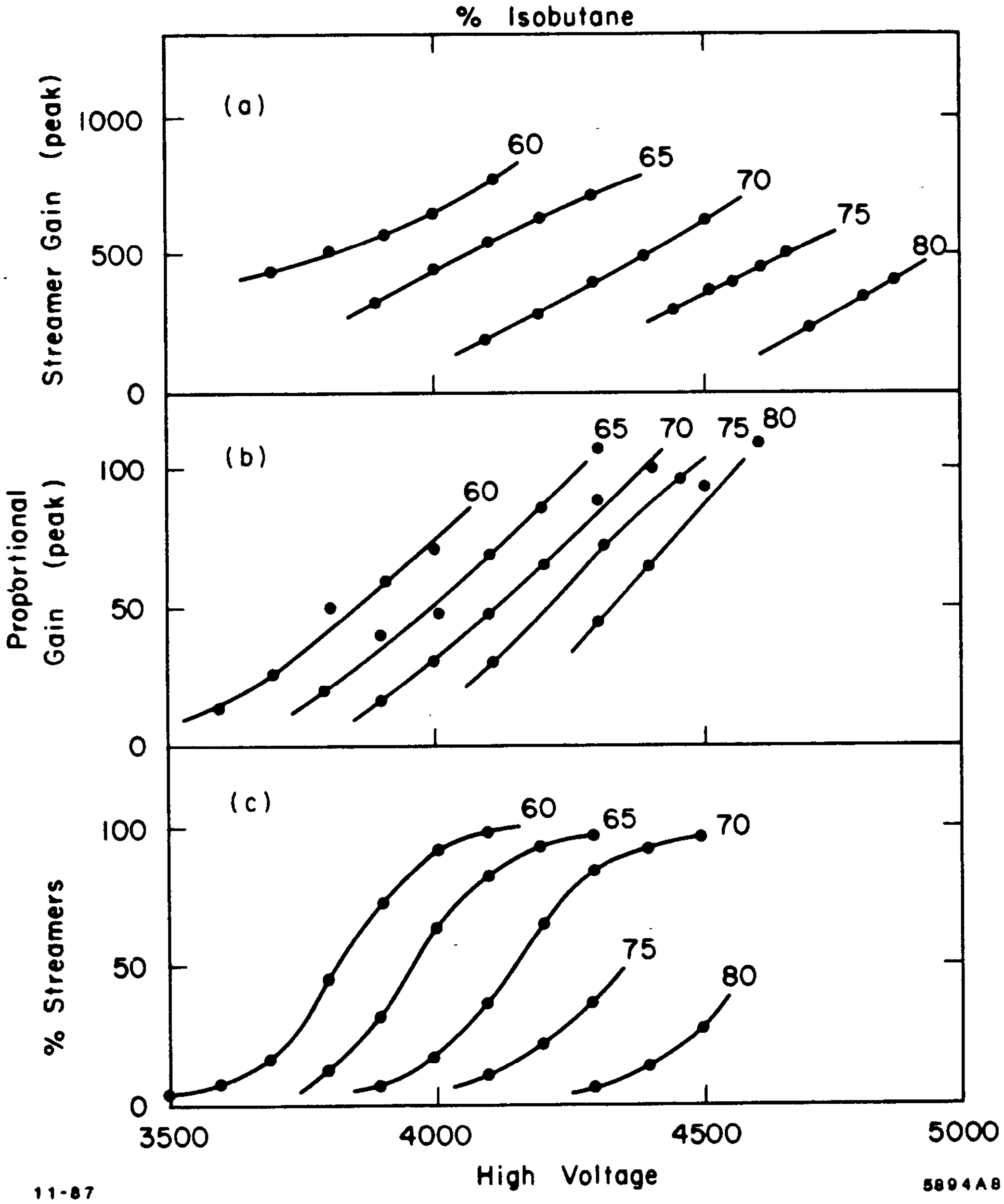
% Isobutane
(a)
Streamer Gain (peak)
1000
500
0
60
65
70
75
80
(b)
Proportional Gain (peak)
100
50
0
60
65
70
75
80
(c)
% Streamers
100
50
0
60
65
70
75
80
3500
4000
4500
5000
High Voltage
11-87
5894A8

Fig. 7

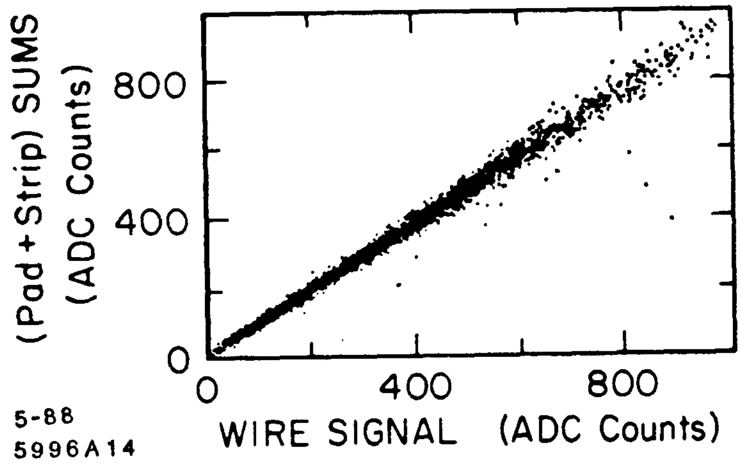

(Pad + Strip) SUMS
(ADC Counts)
800
400
0
0
400
800
5-88
5996A14
WIRE SIGNAL (ADC Counts)

Fig. 8

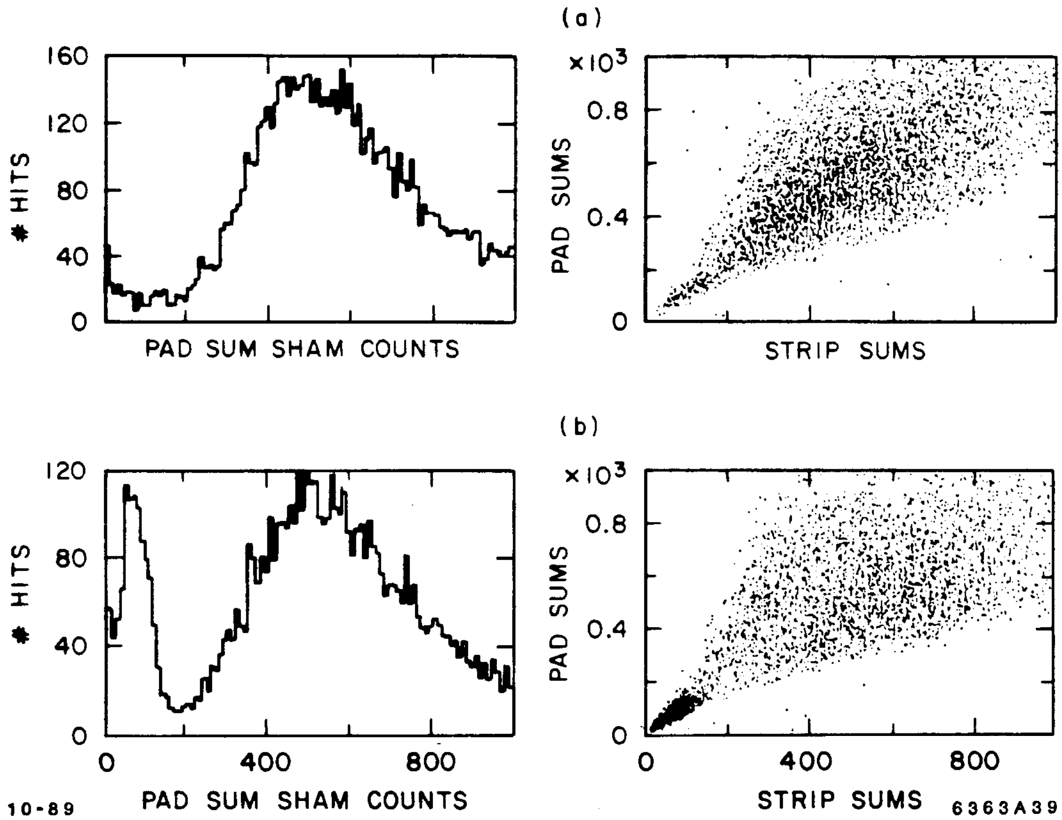
(a)
(b)
160
120
80
40
0
HITS
PAD SUM SHAM COUNTS
×10³
0.8
0.4
PAD SUMS
STRIP SUMS
400
800
10-89
6363A39

Fig. 9

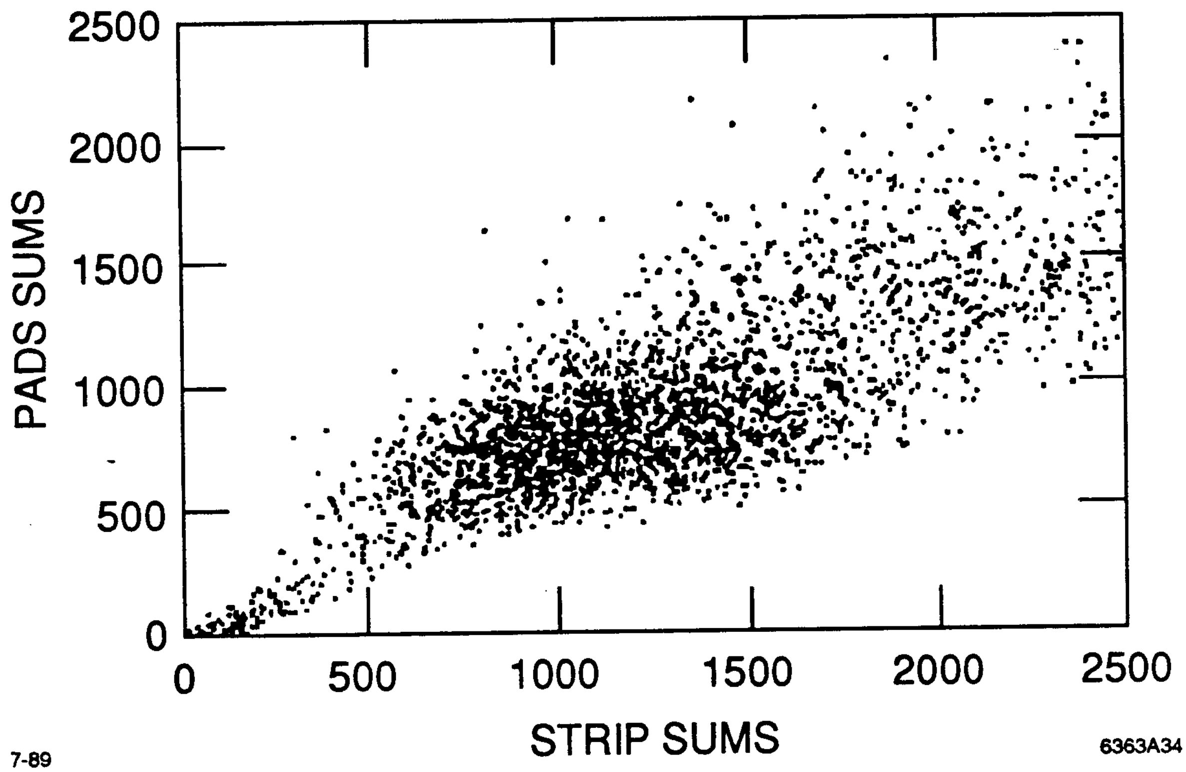
2500
2000
1500
1000
500
0
PADS SUMS
0
500
1000
1500
2000
2500
STRIP SUMS
7-89
6363A34

Fig. 10

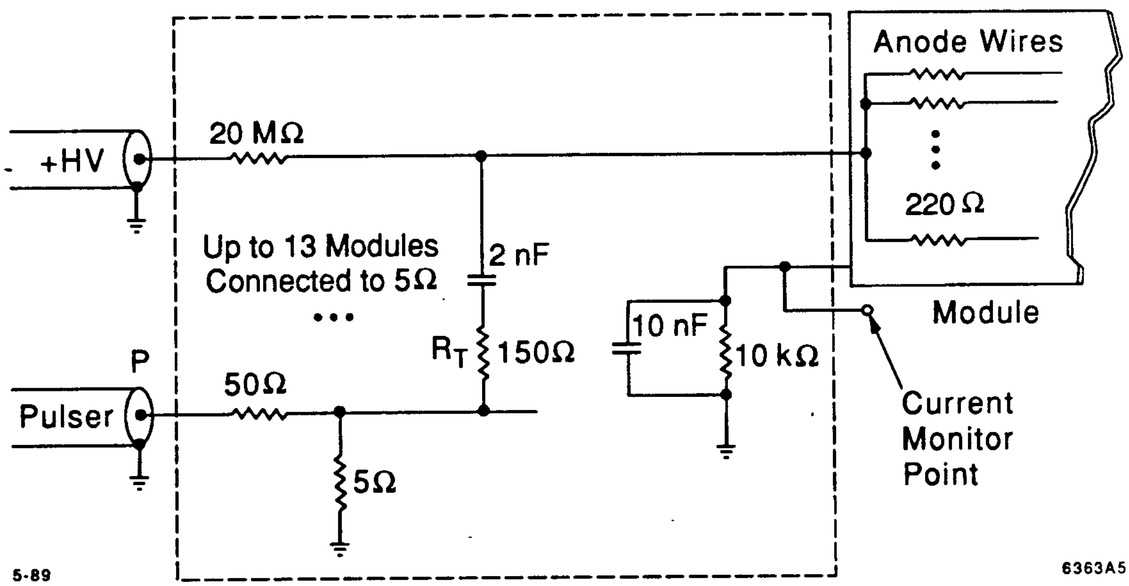
Anode Wires
+HV
20 MΩ
220 Ω
Up to 13 Modules
Connected to 5Ω
2 nF
R_T
150Ω
10 nF
10 kΩ
Module
P
Pulser
50Ω
5Ω
Current
Monitor
Point
5-89
6363A5

Fig. 11

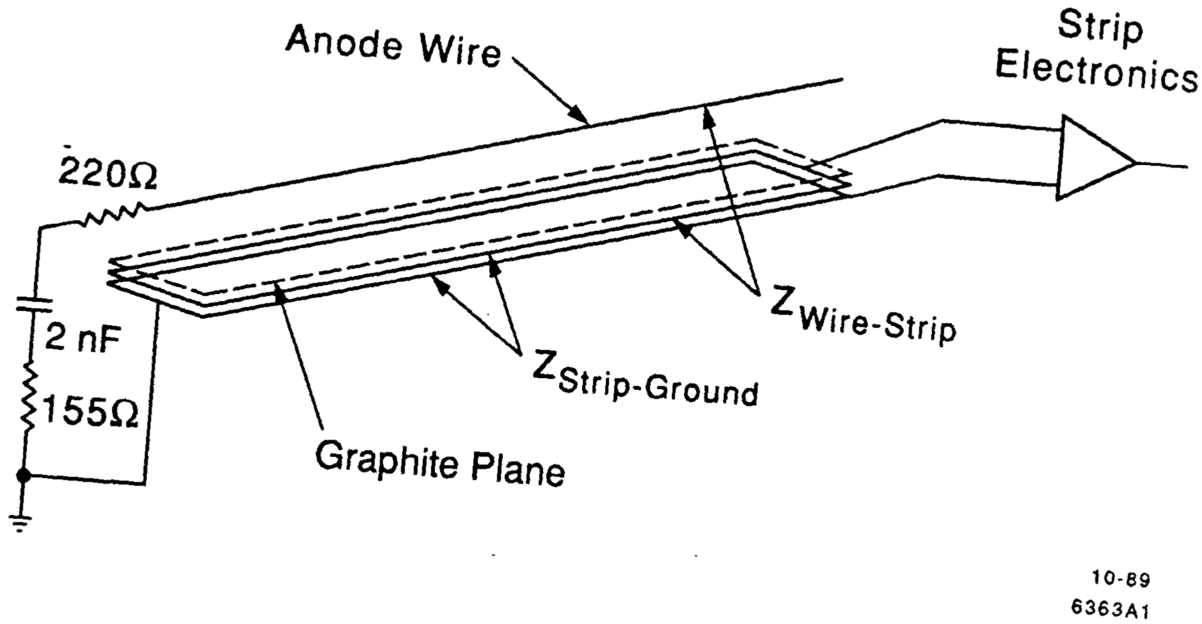
Anode Wire
Strip
Electronics
220Ω
2 nF
155Ω
$Z_{Wire\text{-}Strip}$
$Z_{Strip\text{-}Ground}$
Graphite Plane
10-89
6363A1

Fig. 12

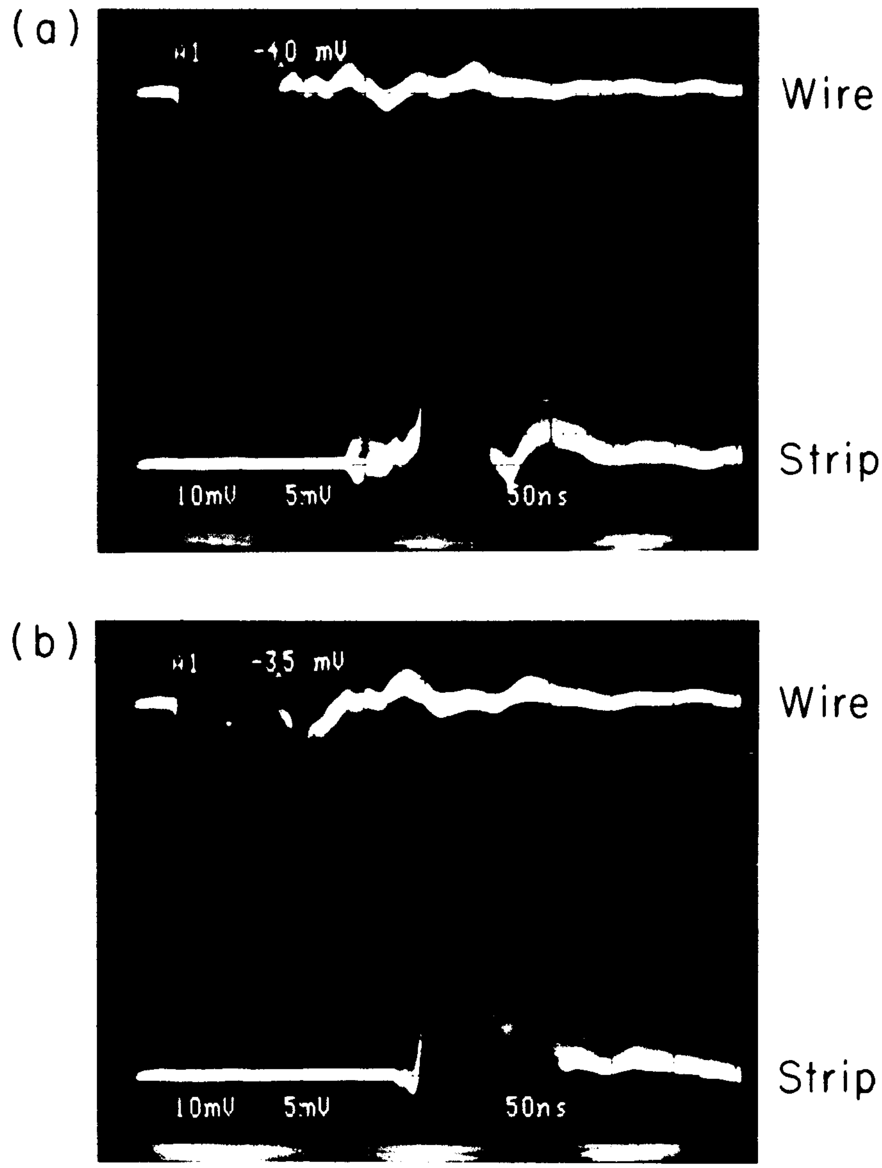

6-89

6363A10

Fig. 13

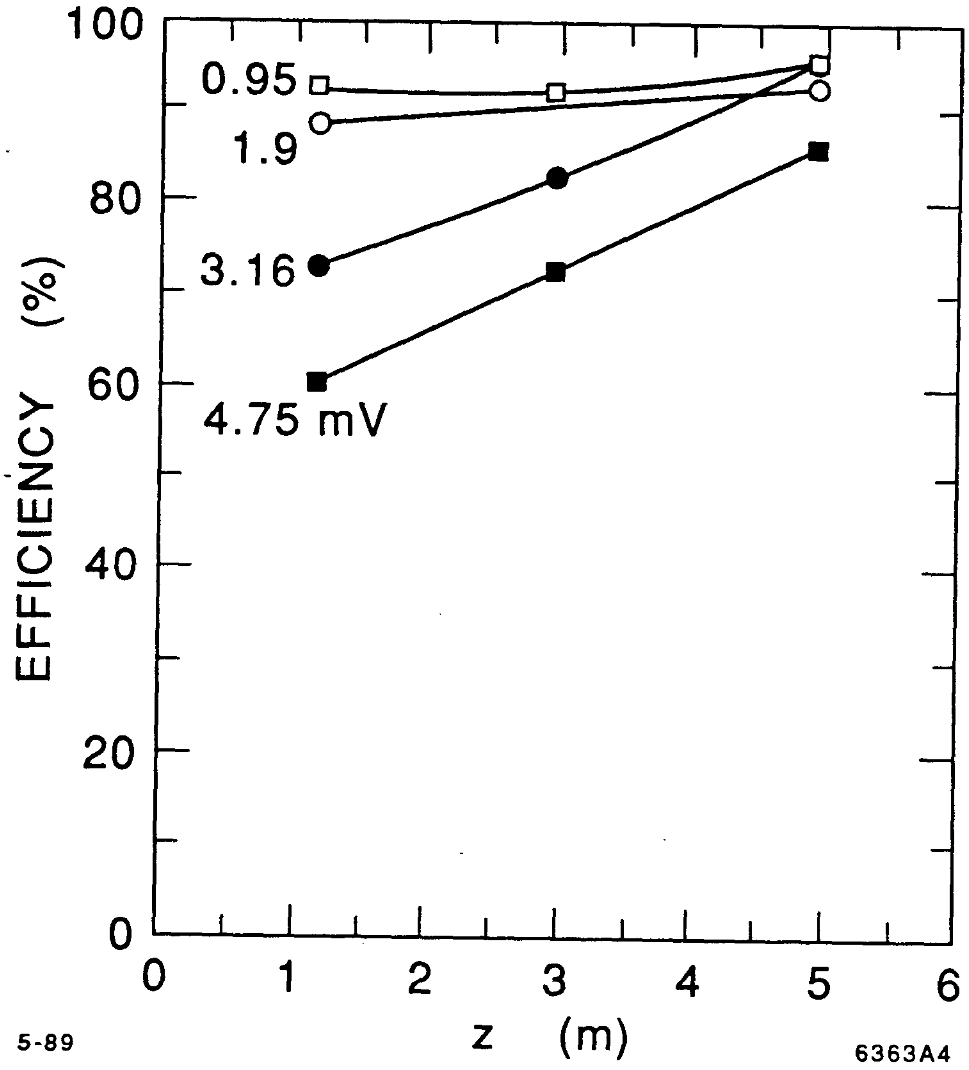

100
80
60
40
20
0
0
1
2
3
4
5
6
EFFICIENCY (%)
z (m)
0.95
1.9
3.16
4.75 mV
5-89
6363A4

Fig. 14

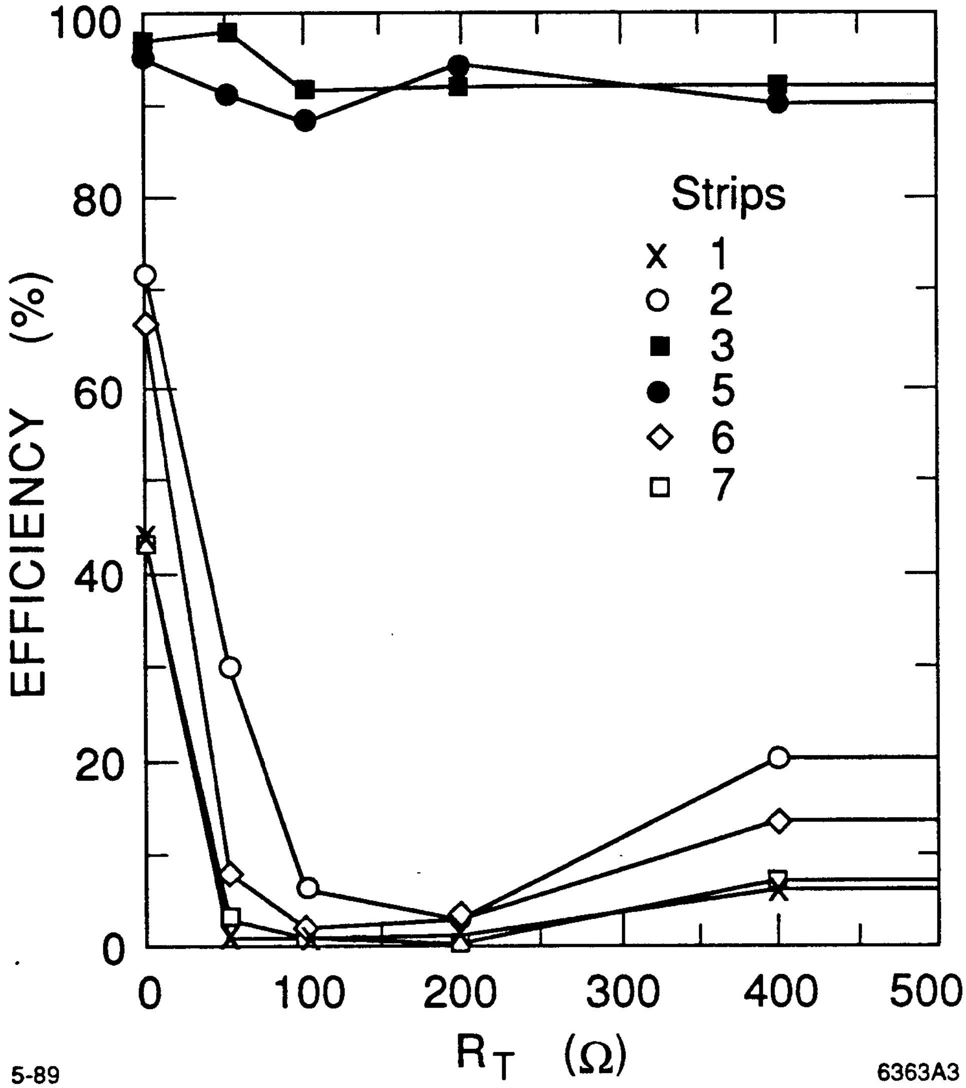

100
80
60
40
20
0
0
100
200
300
400
500
EFFICIENCY (%)
R_T (Ω)
Strips
x 1
○ 2
■ 3
● 5
◇ 6
□ 7
5-89
6363A3

Fig. 15

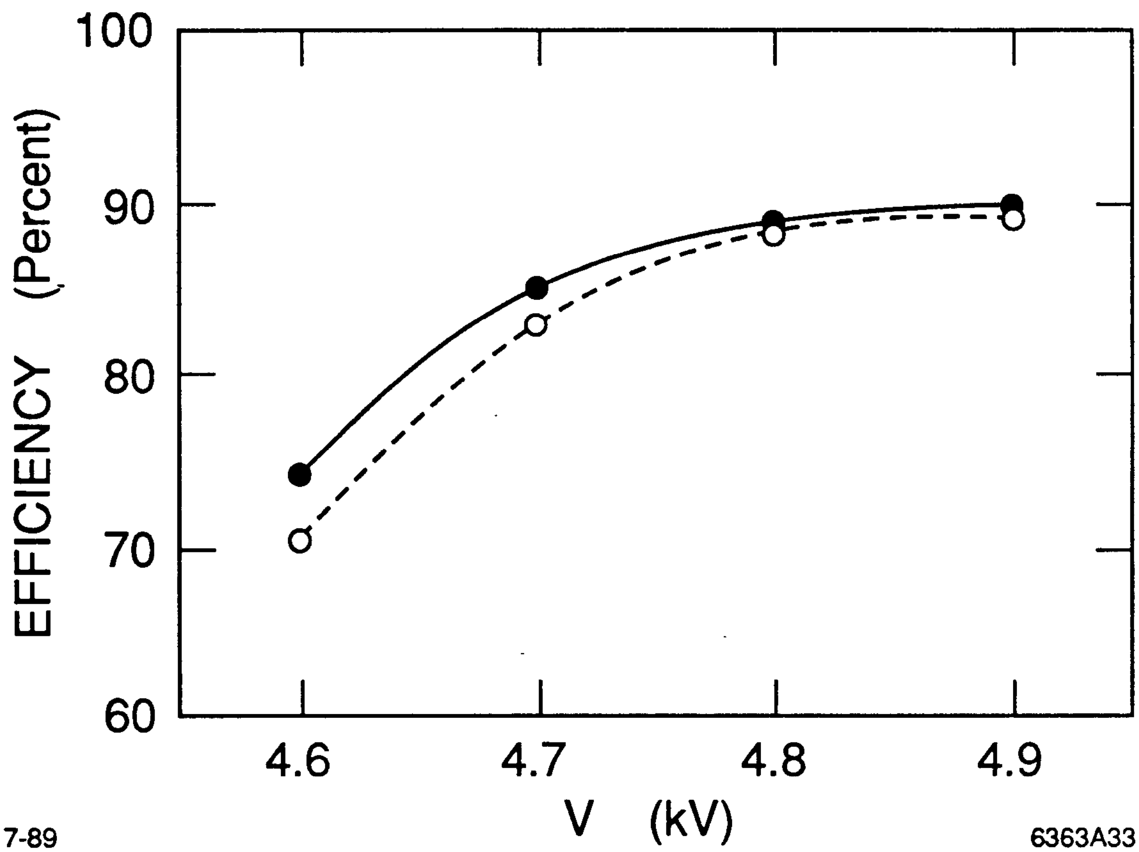

Fig. 16

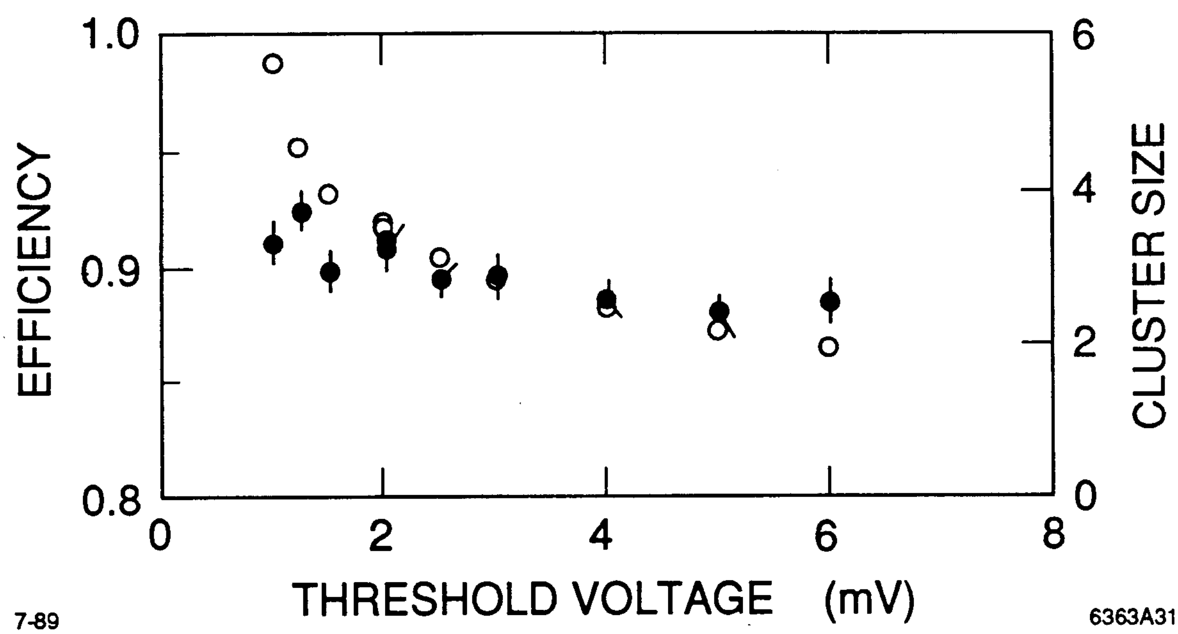
1.0
0.9
0.8
EFFICIENCY
6
4
2
0
CLUSTER SIZE
0
2
4
6
8
THRESHOLD VOLTAGE (mV)
7-89
6363A31

Fig. 17

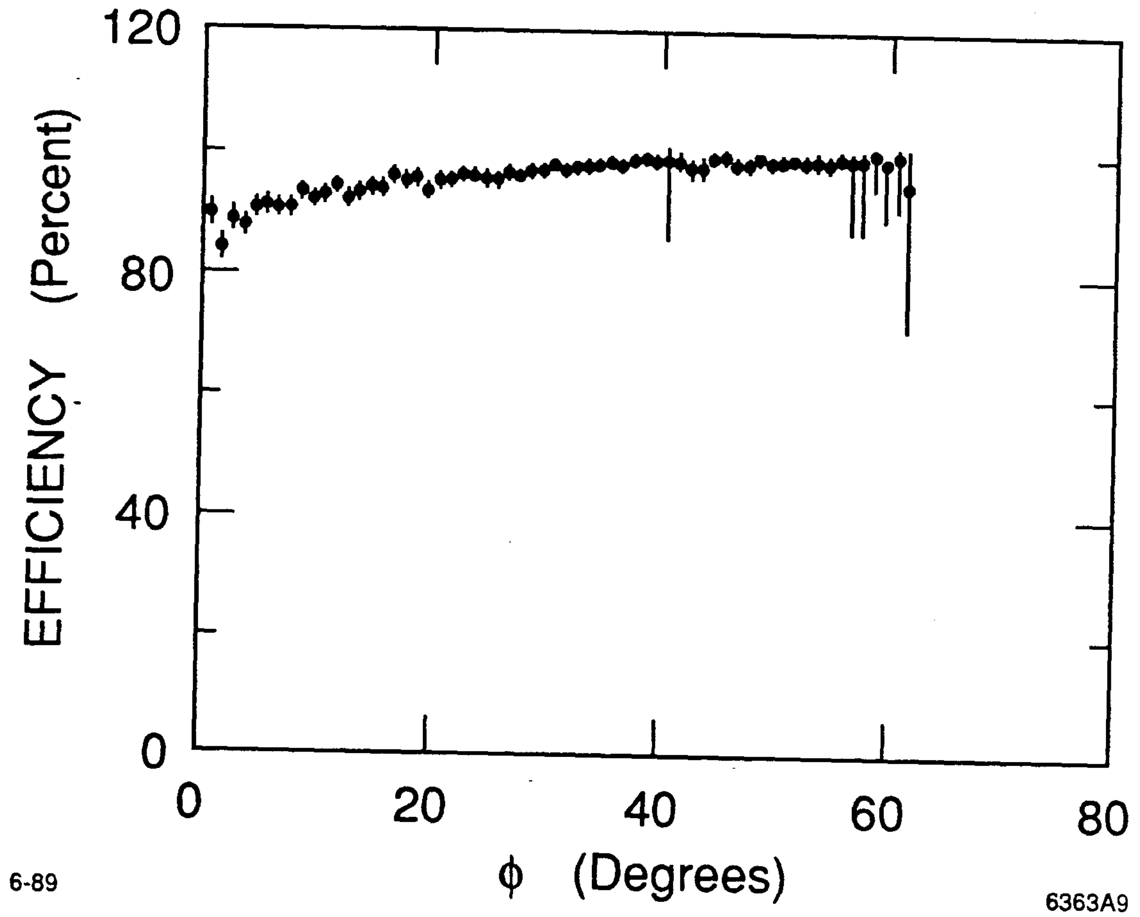

120
80
40
0
EFFICIENCY (Percent)
0
20
40
60
80
φ (Degrees)
6-89
6363A9

Fig. 18

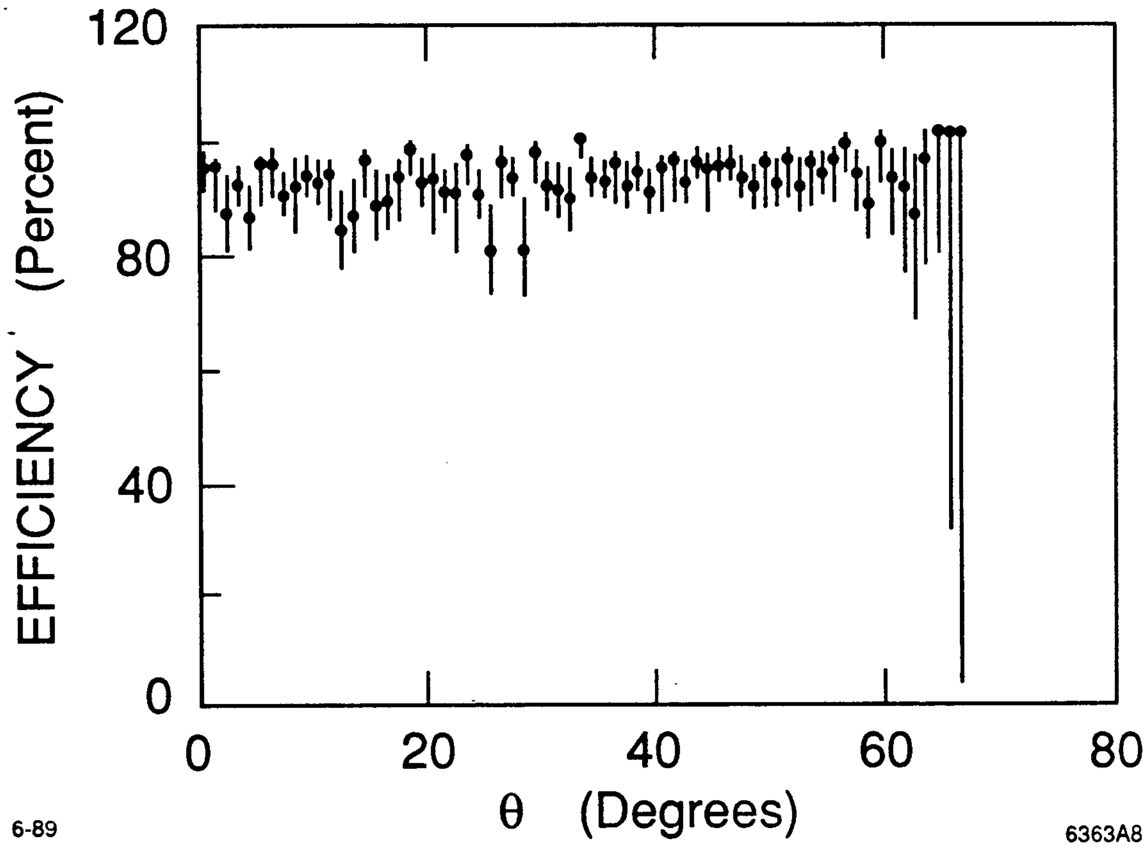
120
80
40
0
EFFICIENCY (Percent)
0
20
40
60
80
θ (Degrees)
6-89
6363A8

Fig. 19

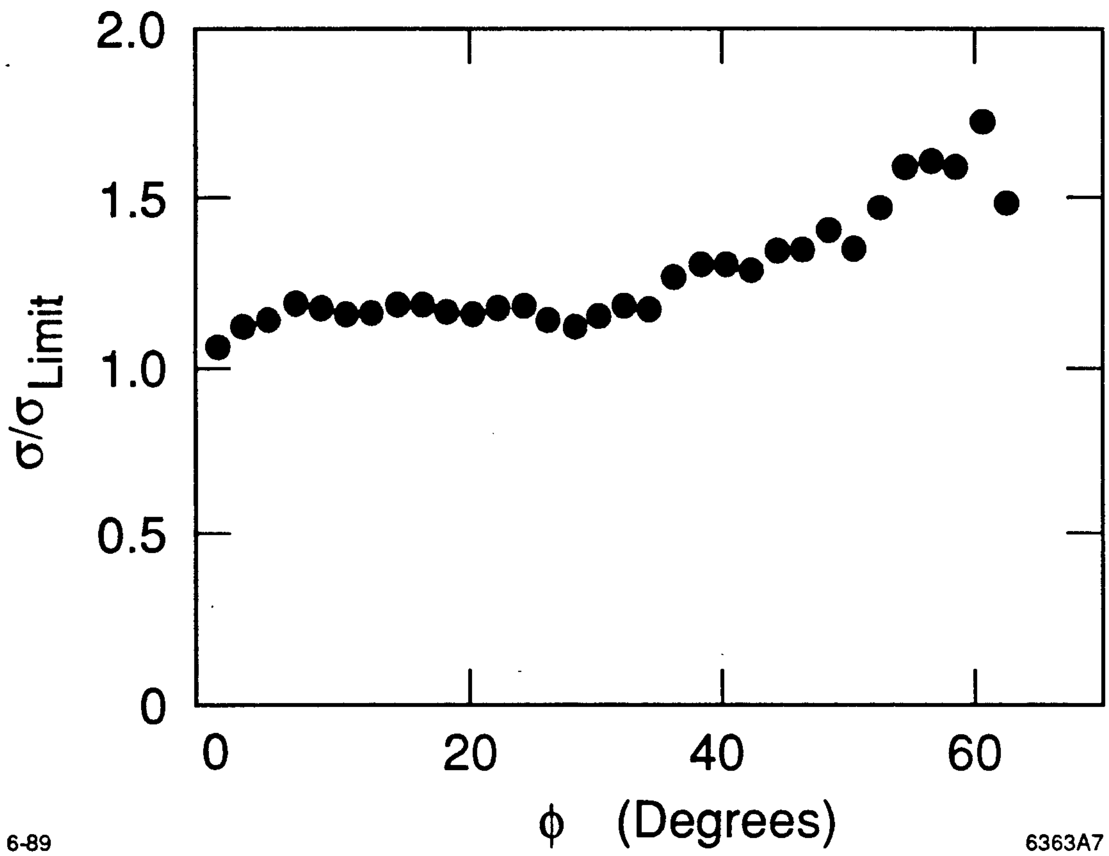
2.0
1.5
1.0
0.5
0
σ/σ_{Limit}
0
20
40
60
ϕ (Degrees)
6-89
6363A7

Fig. 20

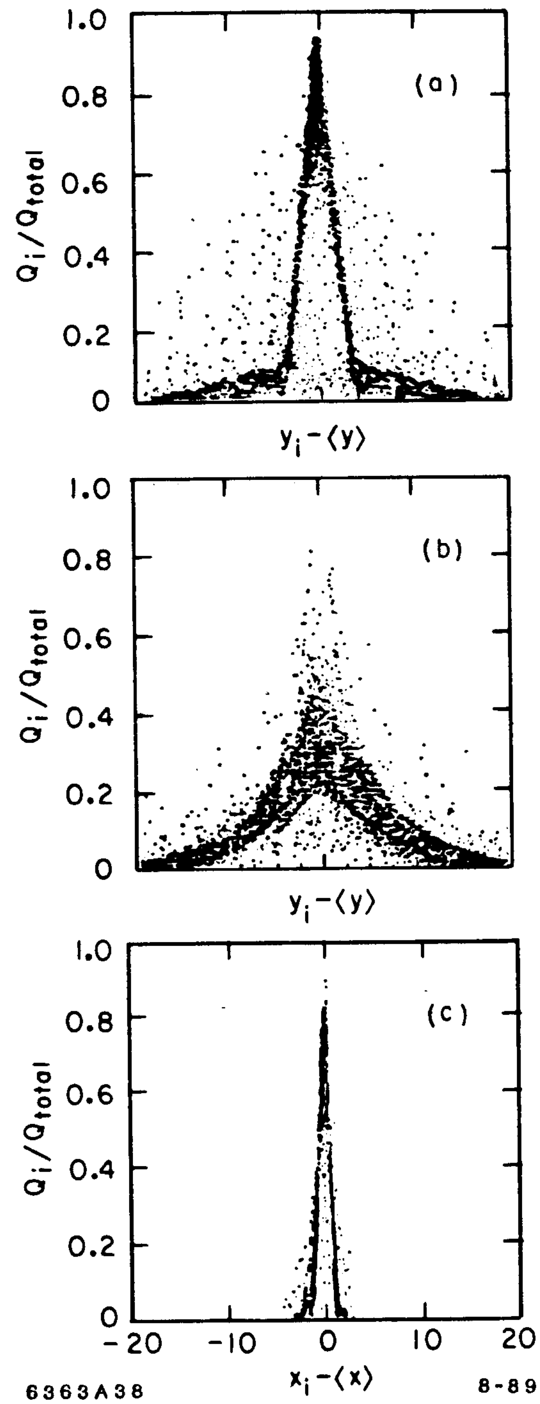
1.0
0.8
0.6
0.4
0.2
0
(a)
Q_i/Q_{total}
$y_i-\langle y\rangle$
(b)
(c)
-20
-10
0
10
20
$x_i-\langle x\rangle$
6363A38
8-89

Fig 21

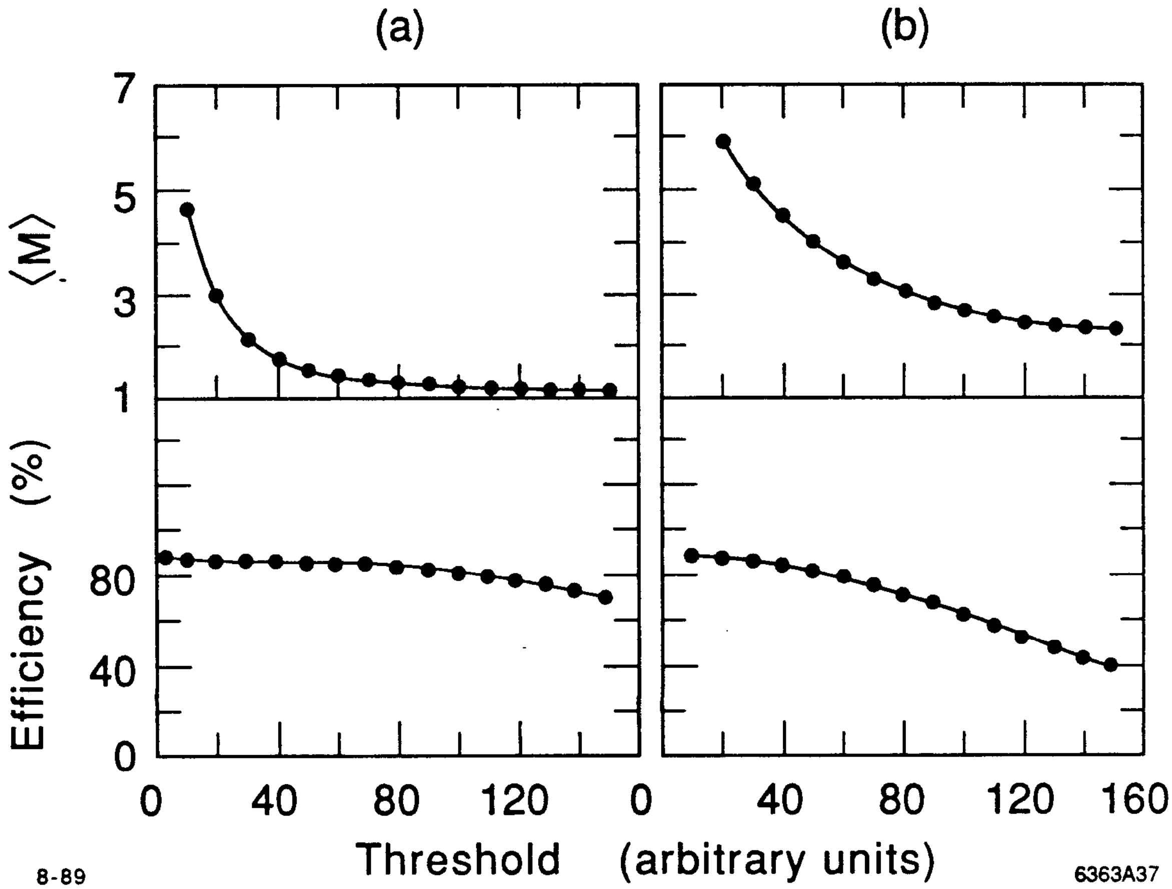

(a)
(b)
7
5
3
1
⟨M⟩
80
40
0
Efficiency (%)
0
40
80
120
0
40
80
120
160
Threshold (arbitrary units)
8-89
6363A37

Fig. 22

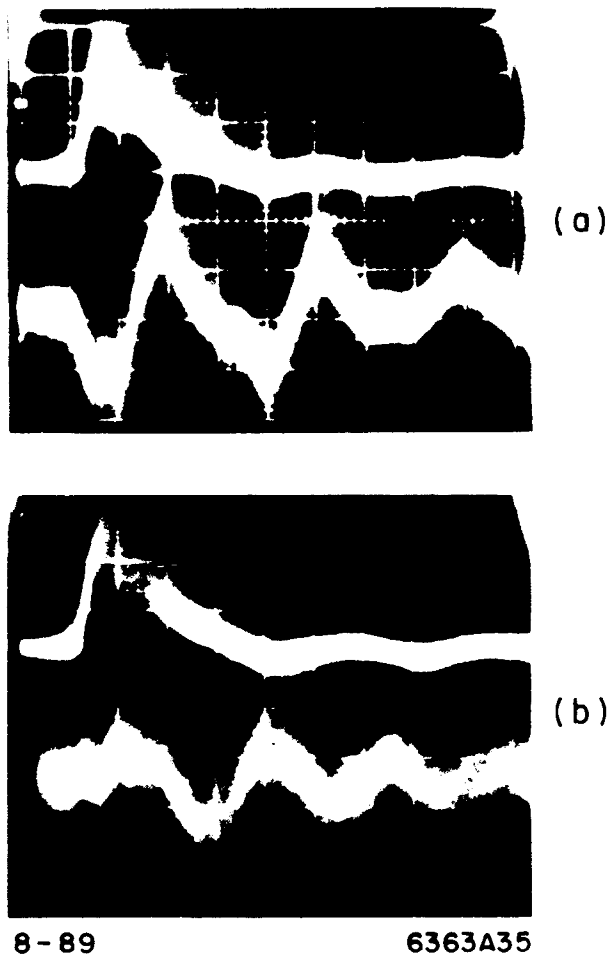

Fig. 23

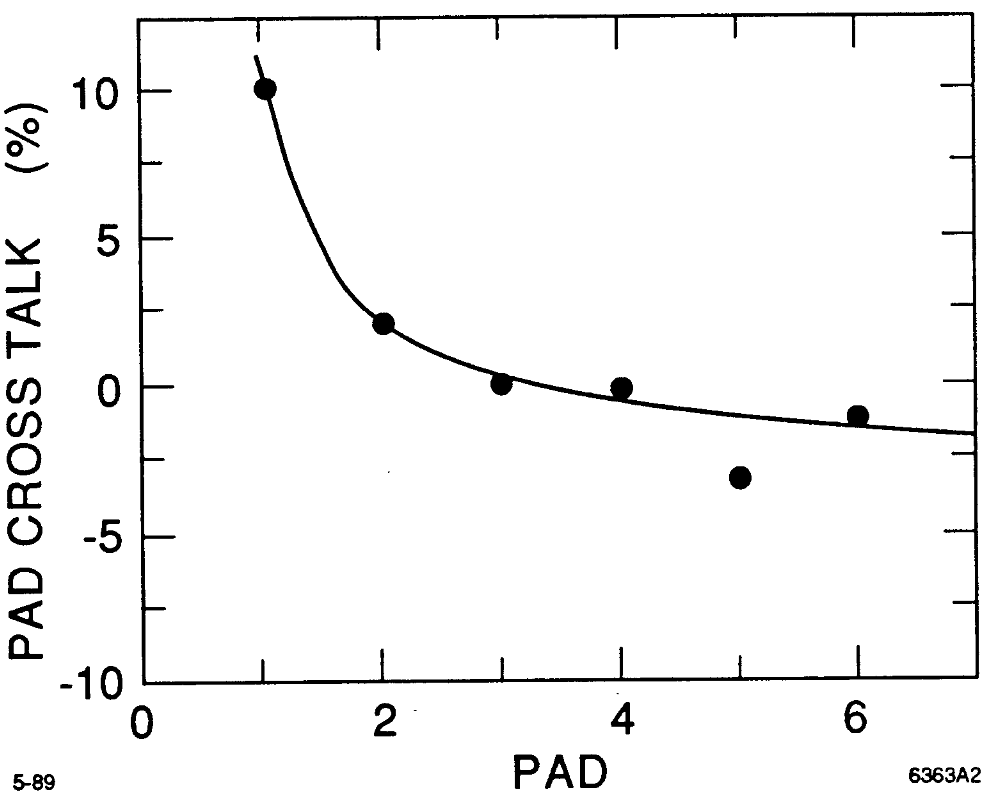

Fig. 24

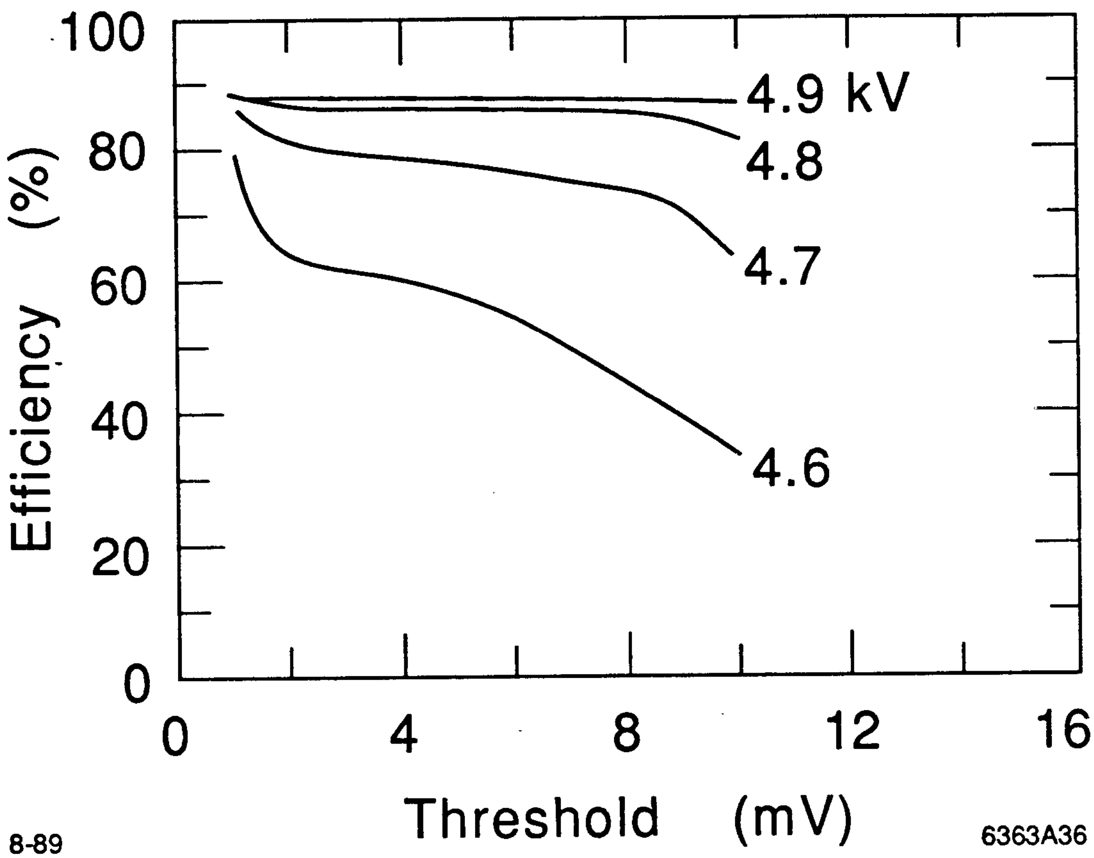

100
80
60
40
20
0
0
4
8
12
16
Efficiency (%)
Threshold (mV)
4.9 kV
4.8
4.7
4.6
8-89
6363A36

Fig. 25

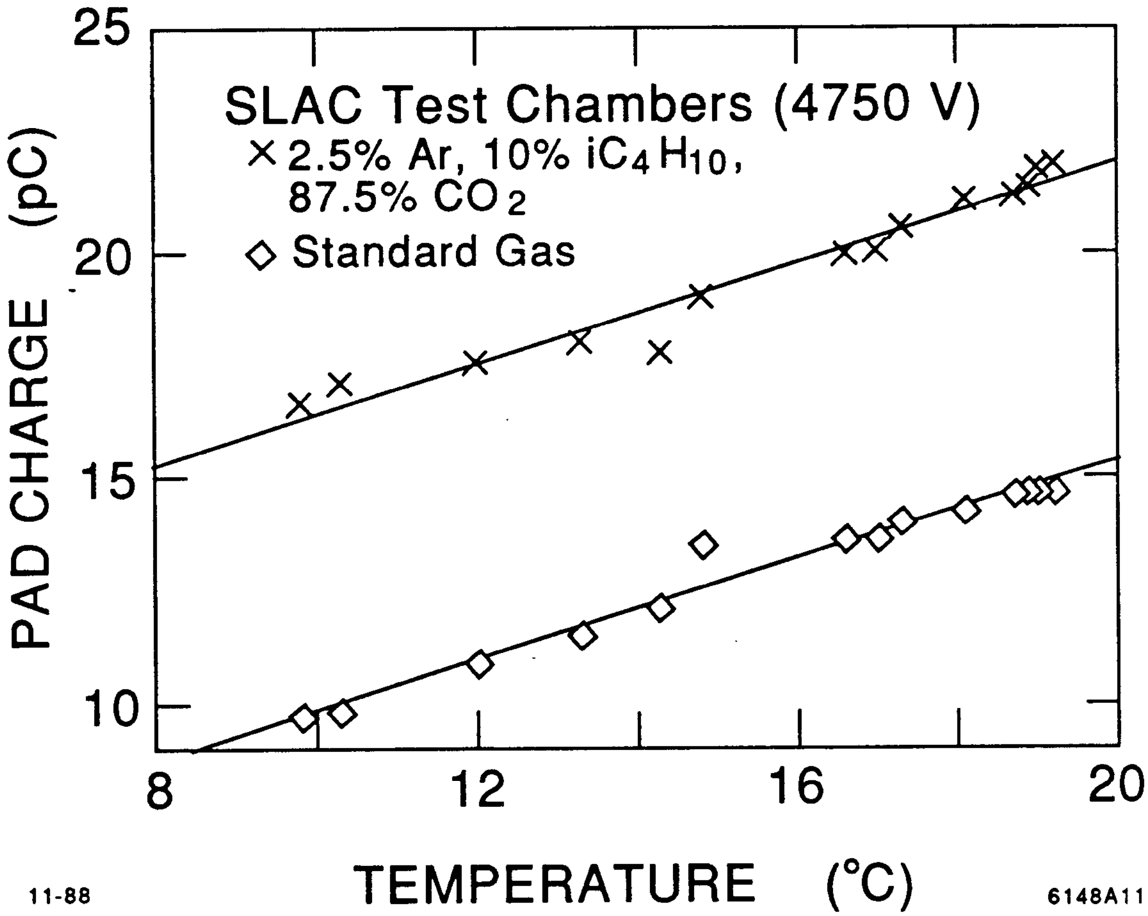

SLAC Test Chambers (4750 V)
× 2.5% Ar, 10% iC4 H10,
87.5% CO2
◇ Standard Gas
PAD CHARGE (pC)
TEMPERATURE (°C)
25
20
15
10
8
12
16
20
11-88
6148A11

Fig. 26

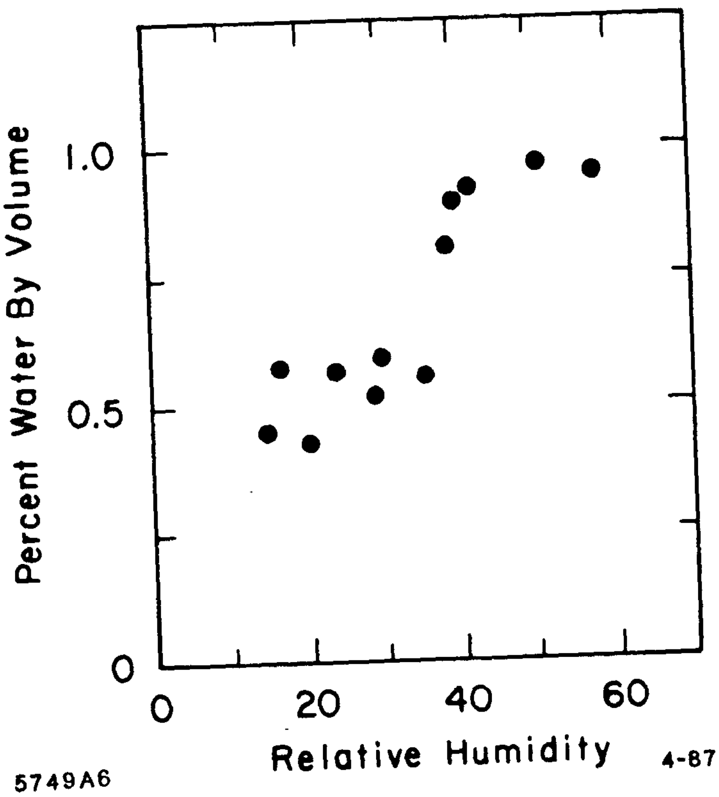
Percent Water By Volume
1.0
0.5
0
0
20
40
60
Relative Humidity
4-87
5749A6

Fig. 27

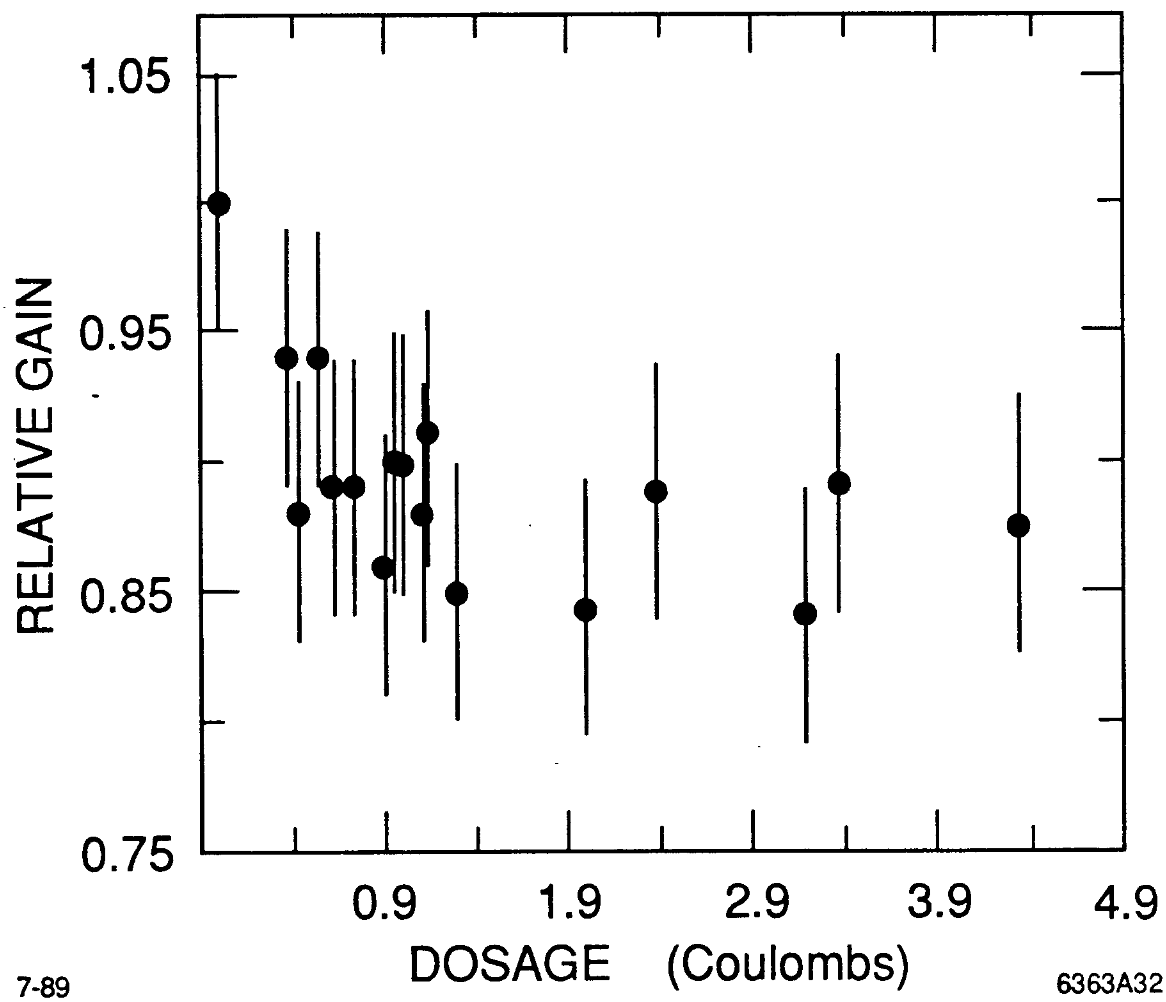

1.05
0.95
0.85
0.75
RELATIVE GAIN
0.9
1.9
2.9
3.9
4.9
DOSAGE (Coulombs)
7-89
6363A32

Fig. 28